

Dark photon and dark Z mediated B meson decays

Alakabha Datta,^a A. Hammad,^b Danny Marfatia,^c Lopamudra Mukherjee,^a and Ahmed Rashed^d

^a*Department of Physics and Astronomy, 108 Lewis Hall, University of Mississippi, Oxford, MS 38677-1848, USA.*

^b*Institute of Convergence Fundamental Studies, Seoul National University of Science and Technology, 232 Gongneung-ro, Nowon-gu, Seoul, 01811, Korea.*

^c*Department of Physics and Astronomy, University of Hawaii at Manoa, 2505 Correa Rd., Honolulu, HI 96822, USA.*

^d*Department of Physics, Shippensburg University of Pennsylvania, Franklin Science Center, 1871 Old Main Drive, Pennsylvania, 17257, USA.*

E-mail: datta@phy.olemiss.edu, ahmed.hammad@uniban.ch,
dmarf8@hawaii.edu, lmukherj@olemiss.edu, amrashed@ship.edu

ABSTRACT: We study flavor changing neutral current decays of B and K mesons in the dark $U(1)_D$ model, with the dark photon/dark Z mass between 10 MeV and 2 GeV. Although the model provides an improved fit (compared to the standard model) to the differential decay distributions of $B \rightarrow K^{(*)}\ell^+\ell^-$, with $\ell = \mu, e$, and $B_s \rightarrow \phi\mu^+\mu^-$, the allowed parameter space is ruled out by measurements of atomic parity violation, $K^+ \rightarrow \mu^+ + \text{invisible}$ decay, and $B_s - \bar{B}_s$ mixing, among others. To evade constraints from low energy data, we extend the model to allow for (1) additional invisible Z_D decay, (2) a direct vector coupling of Z_D to muons, and (3) a direct coupling of Z_D to both muons and electrons, with the electron coupling fine-tuned to cancel the Z_D coupling to electrons via mixing. We find that only the latter case survives all constraints.

Contents

1	Introduction	1
2	Formalism	2
2.1	Partonic amplitude of FCNC processes	3
2.2	Semileptonic FCNC amplitudes	4
2.3	Dark boson decay width	5
3	Models	6
4	Constraints	7
4.1	B_s mixing	7
4.2	$B_s \rightarrow \mu^+ \mu^-$	8
4.3	$B \rightarrow K^{(*)} \nu \bar{\nu}$	9
4.4	Kaon decay and mixing	10
4.5	Radiative $K^+ \rightarrow \mu^+ \nu_\mu Z_D$ decays	11
4.6	Radiative $\pi^+ \rightarrow \mu^+ \nu_\mu Z_D$ decays	13
4.7	Atomic parity violation	14
4.8	Neutrino trident and $CE\nu NS$	15
4.9	Collider and other bounds	16
5	Parameter fits	17
5.1	Case A	19
5.2	Case B	19
5.3	Case C	21
6	Muon anomalous magnetic moment	22
7	Summary	23
A	Form factors	24
B	Hadronic loop contributions	26

1 Introduction

Flavor changing neutral currents (FCNCs) are sensitive probes of new physics (NP) and can strongly constrain many extensions of the standard model (SM). In this work we focus on how the wealth of recent FCNC measurements in the B system constrain models with a light gauge boson. We study the dark $U(1)_D$ model which gives rise to a dark photon or a

dark Z in specific circumstances. If only kinetic mixing between the $U(1)_D$ gauge boson and the electromagnetic field strength tensor occurs, then it is a dark photon with purely vector couplings to all SM fermions except neutrinos [1]. If the dark vector boson also has mass mixing with SM gauge fields, then it is a dark Z , often called a Z' [2, 3]. We collectively denote a dark photon and a dark Z by Z_D . In either case, FCNC processes are generated through loops, and as in the SM, the loops are enhanced for up-type quarks because the large top quark mass suppresses the GIM mechanism. In the case of D decays, the quarks in the loop are down type, which suppresses FCNC decays. Hence, we concentrate on FCNC B and K decays.

A characteristic feature of models with light mediators is that the new physics cannot be integrated out, resulting in q^2 dependent Wilson coefficients (WCs). The role of light mediators in FCNC $b \rightarrow s\ell^+\ell^-$ transitions has been discussed extensively [4–15]. In this paper we study a light vector mediator Z_D with mass $0.01 \lesssim M_{Z_D}/\text{GeV} \lesssim 2$ and allow for onshell as well as off shell effects in Z_D decay. We calculate rates for FCNC processes for both the dark photon and dark Z models.¹ Further, we include hadronic decays of the vector boson in estimating its width. We study extensions of the model with direct interactions of Z_D with muons, and with muons and electrons, apart from mixing induced couplings. We also allow for an additional invisible decay of Z_D which could arise from Z_D couplings to dark sector particles.

The paper is organized as follows. In Section 2 we discuss the general formalism of FCNC B and K decays in the dark photon and the dark Z models. The Wilson coefficients pertaining to $b \rightarrow s\ell^+\ell^-$ and the treatment of the new physics branching fractions in the narrow width approximation, are provided. In this section, we also calculate the width of the Z_D boson including decays to leptonic, hadronic and invisible states. In Section 3 we describe our three model cases and place experimental constraints on them in Section 4. In Section 5, we present the results of our fits to B and K decay data. After a short discussion of the muon anomalous magnetic moment in Section 6, we summarize in Section 7.

2 Formalism

We assume that Z_D is associated with a broken $U(1)_D$ gauge symmetry of a dark sector and couples with the SM gauge symmetry via kinetic mixing between $U(1)_Y$ and $U(1)_D$ [1]. Following Ref. [3] we write the gauge Lagrangian as,

$$\begin{aligned} \mathcal{L}_{\text{gauge}} &= -\frac{1}{4}B_{\mu\nu}B^{\mu\nu} + \frac{1}{2}\frac{\varepsilon}{\cos\theta_W}B_{\mu\nu}Z_D^{\mu\nu} - \frac{1}{4}Z_{D\mu\nu}Z_D^{\mu\nu}, \\ B_{\mu\nu} &= \partial_\mu B_\nu - \partial_\nu B_\mu, \quad Z_{D\mu\nu} = \partial_\mu Z_{D\nu} - \partial_\nu Z_{D\mu}, \end{aligned} \quad (2.1)$$

with ε is a dimensionless parameter and θ_W is the weak mixing angle.

After diagonalizing the gauge sector [3, 17], an induced coupling of Z_D to the SM electromagnetic current is generated. To leading order in ε ,

¹Previously in Ref. [16], flavor changing $b \rightarrow sZ_D$ processes were studied without including the contribution from the q^2 independent dark Z monopole operator. Consequently, $\mathcal{O}(1)$ mixing parameters were incorrectly obtained from $b \rightarrow s\ell^+\ell^-$ data.

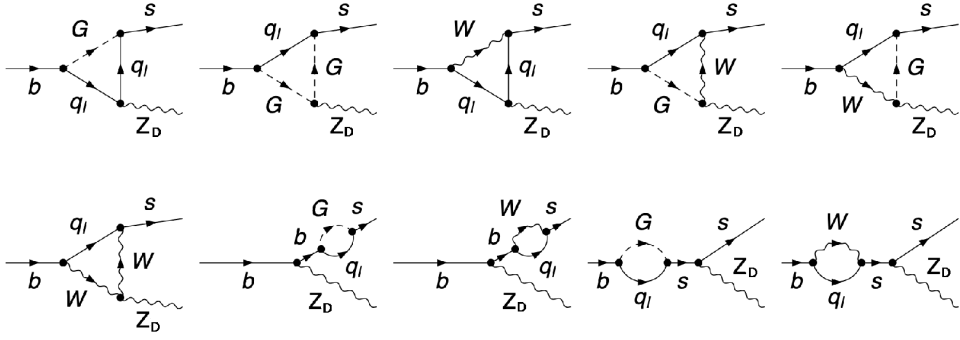


Figure 1. Feynman diagrams for the FCNC process $b \rightarrow s Z_D$ at the parton level. G denotes Goldstone bosons.

$$\mathcal{L}_D^{\text{em}} \supset e \varepsilon Z_D^\mu J_\mu^{\text{em}} - i e \varepsilon [[Z_D W^+ W^-]] , \quad (2.2)$$

where

$$[[Z_D W^+ W^-]] = \varepsilon_{Z_D}^\mu(k_1) \varepsilon_{W^+}^\nu(k_2) \varepsilon_{W^-}^\lambda(k_3) \times [(k_1 - k_2)_\lambda g_{\mu\nu} + (k_2 - k_3)_\mu g_{\nu\lambda} + (k_3 - k_1)_\nu g_{\lambda\mu}] . \quad (2.3)$$

This is the usual *dark photon* model. If the $U(1)_D$ symmetry is broken by a scalar that is charged under the SM, then Z_D can mix with the SM Z boson via mass terms [2, 3]. The physical eigenstates can be written in terms of the weak eigenstates as

$$\begin{aligned} Z &= Z^0 \cos \xi - Z_D^0 \sin \xi , \\ Z_D &= Z^0 \sin \xi + Z_D^0 \cos \xi , \end{aligned} \quad (2.4)$$

where ξ parameterizes the mass mixing between the gauge bosons. This induces a coupling of Z_D with the SM fields given by,

$$\mathcal{L}_D^Z \supset \frac{g}{\cos \theta_W} \varepsilon_Z Z_D^\mu J_\mu^Z - i g \cos \theta_W \varepsilon_Z [[Z_D W^+ W^-]] , \quad (2.5)$$

where $\varepsilon_Z \equiv \frac{1}{2} \tan 2\xi$. Such an interaction defines the *dark Z* model. Note that if $U(1)_D$ is broken by SM singlet scalars, then $\varepsilon_Z = 0$ and we recover the special case of a dark photon. We do not consider a specific Higgs sector for the spontaneous symmetry breaking of $U(1)_D$, and instead study mass mixing of the general form in Eq. (2.4). Since the gauge kinetic mixing parameter ε affects the mass-mixing angle ξ at subleading order, we neglect its effect. The free parameters of the model are the mixing parameters ε and ε_Z , and the mass of the dark boson M_{Z_D} . Updated allowed values of these parameters can be found in Refs. [18–20].

2.1 Partonic amplitude of FCNC processes

FCNC B and K decays proceed via the underlying quark level transitions $d_i \rightarrow d_j Z_D$, where $d_{i,j}$ are down type quarks. The quark level transitions are $b \rightarrow s$, $b \rightarrow d$ and $s \rightarrow d$.

Since Z_D is flavor conserving, the decay occurs at loop level. The process $d_i \rightarrow d_j Z_D$ can be written in terms of the SM $d_i \rightarrow d_j \gamma$ and $d_i \rightarrow d_j Z$ processes by modifying the couplings to include the kinetic and mass mixing parameters (ε , ε_Z). The processes can be described by generic effective local operators and their Wilson coefficients. The monopole operators, which conserve chirality, are

$$H_{\text{eff}} \supset (\bar{F}'_a \gamma^\mu P_{L,R} F_b) \left[\left(E_{a,b}^{0,c} \right)_{L,R} g^{\mu\nu} + (g^{\mu\nu} q^2 - q^\mu q^\nu) \left(E_{a,b}^{2,c} \right)_{L,R} \right] V_\nu^c, \quad (2.6)$$

and the dipole operators, which flip chirality, are

$$H_{\text{eff}} \supset (\bar{F}'_a \sigma^{\mu\nu} P_{L,R} F_b q_\mu V_\nu^c) \left(M_{a,b}^{1,c} \right)_{L,R}, \quad (2.7)$$

where $P_{L,R} = (1/2)(1 \mp \gamma^5)$ are the projection operators, the metric tensor is defined as $g^{\mu\nu} = \text{diag}(1, -1, -1, -1)$, $\sigma^{\mu\nu} \equiv (i/2) [\gamma^\mu, \gamma^\nu]$, and q^μ is the outgoing momentum of a neutral vector boson V . Fermions of different families are denoted by F and F' , and a , b , c are color indices. Note that in Ref. [16], the first term in Eq. (2.6) which provides the leading contribution for a dark Z , is neglected.

In the above basis of the effective Hamiltonian, the hadronic part of the amplitude involving different Lorentz structures is given by

$$\begin{aligned} \mathcal{M}_{Z_D} = & \langle \mathcal{H}_2 | \bar{d}_i \gamma_\mu P_{L/R} d_j | \bar{\mathcal{H}}_1 \rangle \left[\{ (E_{c_1, c_2}^{0,A})_{L/R} + (E_{c_1, c_2}^{0,Z})_{L/R} \} g^{\mu\nu} \right. \\ & + \{ (E_{c_1, c_2}^{2,A})_{L/R} + (E_{c_1, c_2}^{2,Z})_{L/R} \} (g^{\mu\nu} q^2 - q^\mu q^\nu) \left. \right] V_\nu^{Z_D} \\ & + \langle \mathcal{H}_2 | \bar{d}_i i q_\mu \sigma^{\mu\nu} P_{L/R} d_j | \bar{\mathcal{H}}_1 \rangle \{ (M_{c_1, c_2}^{1,A})_{L/R} + (M_{c_1, c_2}^{1,Z})_{L/R} \} V_\nu^{Z_D}, \end{aligned} \quad (2.8)$$

with $V_\nu^{Z_D}$ is the polarization vector of Z_D and the hadronic currents are provided in Appendix A. We use the `Peng4BSM@LO` package [21] to calculate the amplitudes of $b \rightarrow s Z_D$, $s \rightarrow d Z_D$, and $b \rightarrow d Z_D$ that arise from penguin diagrams; see Fig. 1. The loop functions are calculated to first order in the small masses and momenta of the external fermions. The contribution of the monopole terms dominates over the dipole terms. Expressions for the various loop factors of the triangle diagrams are given in Appendix B.

2.2 Semileptonic FCNC amplitudes

Semileptonic $b \rightarrow s \ell^+ \ell^-$ processes are described by the effective Hamiltonian,

$$\mathcal{H}_{\text{eff}}^{bs\ell\ell} = -\frac{4G_F}{\sqrt{2}} \frac{e^2}{16\pi^2} V_{tb} V_{ts}^* \sum_i (C_i \mathcal{O}_i + C'_i \mathcal{O}'_i), \quad (2.9)$$

where $C_i^{(\prime)}$ are the WCs corresponding to the dimension six operators $\mathcal{O}_i^{(\prime)}$. The operators relevant to our study are $\mathcal{O}_9 = (\bar{s}_L \gamma^\mu b_L)(\bar{\ell} \gamma_\mu \ell)$ and $\mathcal{O}_{10} = (\bar{s}_L \gamma^\mu b_L)(\bar{\ell} \gamma_\mu \gamma_5 \ell)$ and their primed counterparts, which are obtained by flipping the chirality $L \rightarrow R$.

To calculate the WC for the $b \rightarrow s \ell^+ \ell^-$ transition, we combine the hadronic loop factors of the previous section, with the appropriate leptonic $Z_D \ell \ell$ vertex factor and the

Z_D propagator, to get

$$\begin{aligned} \mathcal{C}_{9,\ell} &= \left[\left((E_{c_1,c_2}^{0,Z})_L + \{ (E_{c_1,c_2}^{2,A})_L + (E_{c_1,c_2}^{2,Z})_L \} q^2 \right) \right. \\ &\quad \times \left. \left(\frac{1}{q^2 - M_{Z_D}^2 + i\Gamma_{Z_D} M_{Z_D}} \right) \left(e\varepsilon + \frac{g}{c_W} \varepsilon_Z g_V^\ell \right) \right], \end{aligned} \quad (2.10)$$

$$\begin{aligned} \mathcal{C}_{10,\ell} &= \left[\left((E_{c_1,c_2}^{0,Z})_L + \{ (E_{c_1,c_2}^{2,A})_L + (E_{c_1,c_2}^{2,Z})_L \} q^2 \right) \right. \\ &\quad \times \left. \left(\frac{1}{q^2 - M_{Z_D}^2 + i\Gamma_{Z_D} M_{Z_D}} \right) \left(\frac{g}{c_W} \varepsilon_Z g_A^\ell \right) \right], \end{aligned} \quad (2.11)$$

$$\mathcal{C}'_{9,\ell} = \mathcal{C}'_{10,\ell} = 0, \quad (2.12)$$

where $g_V^\ell = (-1 + 4s_W^2)/2$ and $g_A^\ell = -1/2$ are the vector and axial vector coupling constants for the SM $Z\ell\ell$ interaction; s_W and c_W are the sine and cosine of θ_W , respectively. When obvious, we suppress the ℓ subscript in the WCs.

If M_{Z_D} is outside the measured q^2 bin, an off-shell contribution to the semileptonic decay amplitude can interfere effect with the SM amplitude. However, if M_{Z_D} lies within a particular q^2 bin, then the new physics contribution can be treated as arising from the on-shell production of the light boson followed by its subsequent decay to lepton pairs ($\mathcal{H}_1 \rightarrow \mathcal{H}_2 Z_D, Z_D \rightarrow \ell^+ \ell^-$). As the width of the light boson is much smaller than the energy resolution of the detector, the narrow width approximation can be employed to write the branching fraction as [9]

$$\langle \mathcal{B} \rangle_{b \rightarrow s \ell \ell}^{q_{min}^{max}} = \langle \mathcal{B} \rangle_{b \rightarrow s \ell \ell}^{SM} |_{q_{min}^{max}} + \mathcal{B}(\mathcal{H}_1 \rightarrow \mathcal{H}_2 Z_D) \mathcal{B}(Z_D \rightarrow \ell^+ \ell^-) \cdot \mathcal{G}^{(r_\ell)}(q_{min}, q_{max}), \quad (2.13)$$

where

$$\mathcal{G}^{(r_\ell)}(q_{min}, q_{max}) = \frac{1}{\sqrt{2\pi} r_\ell} \int_{q_{min}}^{q_{max}} d|q| e^{-\frac{(|q| - M_{Z_D})^2}{2r_\ell^2}}, \quad (2.14)$$

is a Gaussian smearing function with $r_e = 10$ MeV and $r_\mu = 2$ MeV. It is important to note that the on-shell decay of the light boson always enhances the contribution to the branching fraction in a bin.

2.3 Dark boson decay width

In the mass range of interest, Z_D decays to lepton pairs and to hadronic final states. While the e^+e^- and $\nu\bar{\nu}$ final states are always kinematically allowed, the $\mu^+\mu^-$ final state is possible only for $M_{Z_D} > 2m_\mu$. The decay widths to charged and neutral leptons are given by

$$\begin{aligned} \Gamma(Z_D \rightarrow \ell^+ \ell^-) &= \frac{e^2}{96\pi c_W^2 s_W^2 M_{Z_D}} \sqrt{1 - 4\frac{m_\ell^2}{M_{Z_D}^2}} \left(8c_W^2 s_W^2 \varepsilon^2 (2m_\ell^2 + M_{Z_D}^2) \right. \\ &\quad - 4c_W s_W (4s_W^2 - 1) \varepsilon \varepsilon_Z (2m_\ell^2 + M_{Z_D}^2) \\ &\quad \left. + \varepsilon_Z^2 (m_\ell^2 (16s_W^4 - 8s_W^2 - 1) + M_{Z_D}^2 (8s_W^4 - 4s_W^2 + 1)) \right), \end{aligned} \quad (2.15)$$

$$\Gamma(Z_D \rightarrow \nu\bar{\nu}) = \frac{e^2 M_{Z_D} \varepsilon_Z^2}{96\pi c_W^2 s_W^2}. \quad (2.16)$$

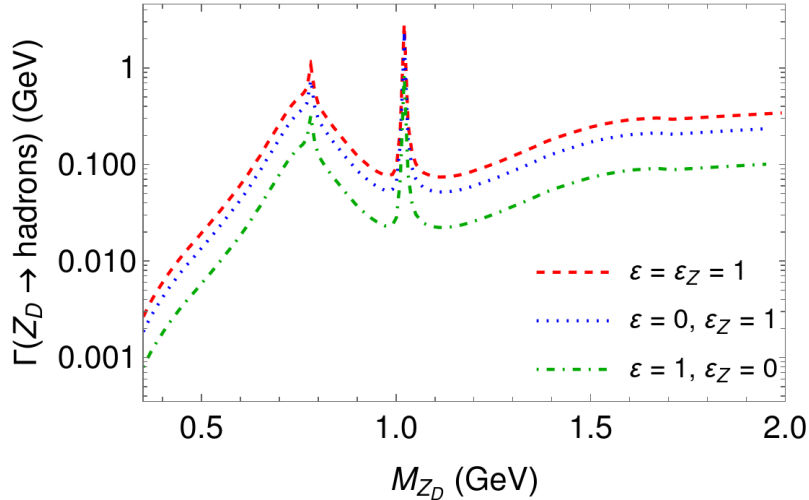


Figure 2. Decay width of the dark boson to light hadronic final states for different mixing parameter values.

Hadronic decays, however, cannot be calculated using perturbative QCD and we rely on the vector meson dominance model (VMD) to describe low energy QCD [22–26]. Recently, the hadronic decay width of light $U(1)$ vector bosons has been calculated in a data driven approach [27–29]. The hadronic decay of a dark photon, with coupling proportional to the electric charge, can be expressed by an appropriate rescaling as

$$\Gamma(Z_D \rightarrow \mathcal{H}) = \Gamma(Z_D \rightarrow \mu^+ \mu^-) \times \mathcal{R}_\mu^{\mathcal{H}} \quad (2.17)$$

where $\mathcal{R}_\mu^{\mathcal{H}} = \sigma(e^+e^- \rightarrow \mathcal{H})/\sigma(e^+e^- \rightarrow \mu^+\mu^-)$ has been experimentally measured [30]. For energies far from the hadron resonances, e^+e^- annihilation slowly transitions towards perturbative quark pair production, in which case $\mathcal{R}_\mu^{\mathcal{H}} \simeq N_c \sum_{f=u,d,s} (Q_{em}^f)^2 = 2$ for SM, where $N_c = 3$ is the color factor and Q_{em}^f is the electromagnetic charge of fermion f . The hadronic decay width of baryophilic dark photons has been computed in Ref. [29] by summing over various hadronic final states in the VMD model. We adapt this analysis to the vector coupling of the dark Z . For the axial vector coupling of Z_D we use quark level decays to estimate the contribution to the hadronic width. In Fig. 2 we show the Z_D partial width to hadronic final states for different mixing parameter values.

3 Models

We study three different cases of the light Z_D model as specified below.

- **Case A:** This is the dark photon and dark Z model described by Eqs. (2.2) and (2.5). The model has two mixing parameters (ε and ε_Z) and the mass M_{Z_D} .
- **Case B:** A muonphilic Z_D in which Case A is extended with an additional direct interaction of the dark Z with muons:

$$\mathcal{L}_D^Z \supset g_D^\mu \bar{\mu} \gamma_\alpha \mu Z_D^\alpha. \quad (3.1)$$

This scenario has an additional free parameter g_D^μ .

- **Case C:** Case A is extended with additional direct interactions of the dark Z with both electrons and muons:

$$\mathcal{L}_D^Z \supset g_D^e \bar{e} \gamma_\alpha e Z_D^\alpha + g_D^\mu \bar{\mu} \gamma_\alpha \mu Z_D^\alpha. \quad (3.2)$$

We assume g_D^e is fine-tuned so that it cancels the coupling of Z_D to electrons via mixing. Then, all observables for the electron mode are described by the SM only.

4 Constraints

4.1 B_s mixing

B meson mixing plays an important role in the search for new physics and provides a strong constraint on our models. In the SM, the mixing has its origin in a box diagram with a W boson and top quark in the loop. The dominant contribution to the mass difference due to $B_s^0 - \bar{B}_s^0$ mixing is given by [31]

$$\Delta M_{B_s}^{SM} = \frac{G_F^2 M_{B_s}}{6\pi^2} M_W^2 (V_{tb} V_{ts}^*)^2 \eta_B f_{B_s}^2 \hat{B}_{B_s} S_0(\bar{m}_t^2/M_W^2), \quad (4.1)$$

where $S_0(x)$ is the Inami-Lim function [32],

$$S_0(x) = \frac{4x - 11x^2 + x^3}{4(1-x)^2} - \frac{3x \ln x}{2(1-x)^2}, \quad (4.2)$$

and $\bar{m}_t = 163.53$ GeV is the \overline{MS} mass of the top quark [33]. Here, $\eta_B \approx 0.551$ is a numerical factor that arises from the leading and next-to-leading order QCD corrections to the box diagram [34]. The long-distance physics in the hadronic matrix element, parametrized by the decay constant f_{B_s} and the bag parameter \hat{B}_{B_s} , is the major source of theoretical uncertainty. The product $f_{B_s} \sqrt{\hat{B}_{B_s}} = 256.1(5.7)$ MeV is obtained from lattice calculations with $N_f = 2 + 1 + 1$ dynamical fermions [35]. The dominant NP correction to the mass difference comes from the monopole operator and is given by [8]

$$\Delta M_{B_s}^{NP} = \frac{1}{3} \frac{1}{M_{B_s}^2 - M_{Z_D}^2} f_{B_s}^2 \hat{B}_{B_s} M_{B_s} \{(E_{b,s}^{0,Z})_L\}^2 \left(1 - \frac{5}{8} \frac{m_b^2}{M_{Z_D}^2}\right). \quad (4.3)$$

Note that $(E_{b,s}^{0,Z})_L$ does not depend on ε at one-loop order.

In the SM, the mass difference is [36]

$$\Delta M_{B_s}^{SM} = (18.4_{-1.2}^{+0.7}) \text{ ps}^{-1}, \quad (4.4)$$

which is in agreement with the experimental measurement [30]

$$\Delta M_{B_s}^{exp} = (17.765 \pm 0.006) \text{ ps}^{-1}. \quad (4.5)$$

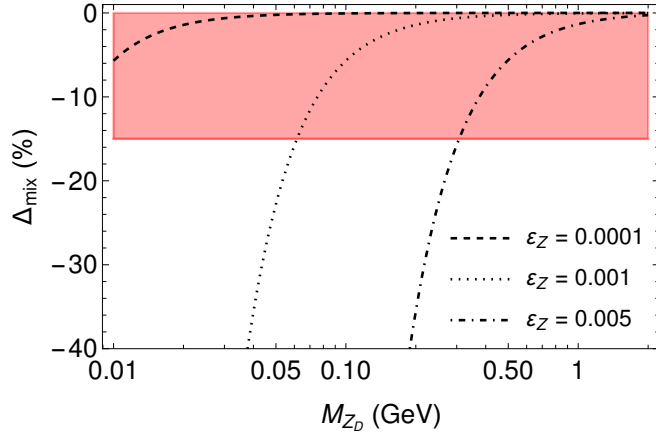


Figure 3. Sensitivity of $B_s^0 - \bar{B}_s^0$ mixing to ε_Z as a function of M_{Z_D} . At leading order Δ_{mix} is independent of ε . The red band is the uncertainty in Δ_{mix} taken to be the 2σ lower uncertainty in $\Delta M_{B_s}^{SM}$.

The total mass difference including the Z_D contribution can be expressed as

$$\Delta M_{B_s} = \Delta M_{B_s}^{SM} + \Delta M_{B_s}^{NP} = \Delta M_{B_s}^{SM} \left(1 + \frac{\Delta M_{B_s}^{NP}}{\Delta M_{B_s}^{SM}} \right) \equiv \Delta M_{B_s}^{SM} (1 + \Delta_{mix}), \quad (4.6)$$

where Δ_{mix} contains the NP information and is free from uncertainties in the decay constant and bag factor. Since $\Delta_{mix} \leq 0$, the 6.5% lower uncertainty in the SM expectation translates into a 6.5% uncertainty in Δ_{mix} . We plot Δ_{mix} as a function of the dark Z mass for different values of ε_Z in Fig. 3. It is evident that lighter Z_D require smaller values of ε_Z for Δ_{mix} to lie within the 2σ uncertainty of the SM prediction. We find that $\varepsilon_Z \gtrsim 0.001$ is disallowed for $M_{Z_D} \lesssim 60$ MeV.

4.2 $B_s \rightarrow \mu^+ \mu^-$

The branching fraction of the rare $B_s \rightarrow \mu^+ \mu^-$ decay, including new physics contributions, is given by

$$\mathcal{B}(B_s \rightarrow \mu^+ \mu^-) = \tau_{B_s} f_{B_s}^2 m_{B_s}^3 \frac{G_F^2 \alpha^2}{64\pi^3} |V_{tb} V_{ts}^*| \sqrt{1 - \frac{4m_\mu^2}{m_{B_s}^2}} \left[\frac{m_{B_s}^2}{m_b^2} \left(1 - \frac{4m_\mu^2}{m_{B_s}^2} \right) |\mathcal{C}_S - \mathcal{C}'_S|^2 + \left| \frac{m_{B_s}}{m_b} (\mathcal{C}_P - \mathcal{C}'_P) + 2 \frac{m_\mu}{m_{B_s}} (\mathcal{C}_{10} - \mathcal{C}'_{10}) \right|^2 \right]. \quad (4.7)$$

In the Z_D model, contributions from the scalar and pseudoscalar WCs, $\mathcal{C}_S^{(\prime)}$ and $\mathcal{C}_P^{(\prime)}$, are absent. The dominant contribution therefore comes from \mathcal{C}_{10} as given in Eq. (2.11). For our numerical estimates we use $f_{B_s} = 230.3(1.3)$ MeV [37]. The SM expectation [38, 39] and experimental measurements are [40]

$$\mathcal{B}(B_s^0 \rightarrow \mu^+ \mu^-)^{SM} = (3.67 \pm 0.15) \times 10^{-9}, \quad (4.8)$$

$$\mathcal{B}(B_s^0 \rightarrow \mu^+ \mu^-)^{LHCb \ 2021} = (3.09_{-0.43}^{+0.46+0.15}) \times 10^{-9}. \quad (4.9)$$

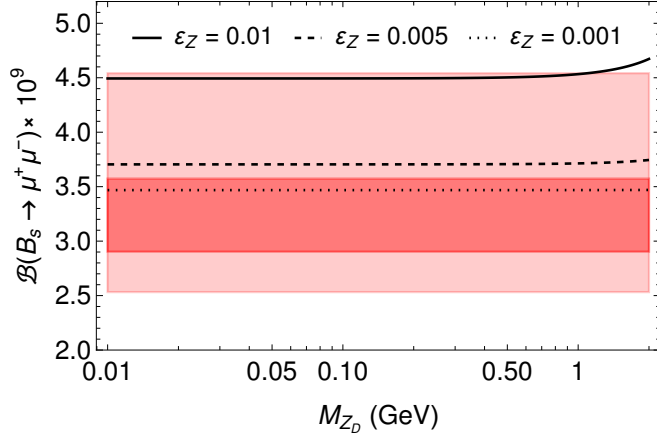


Figure 4. Branching fraction for $B_s \rightarrow \mu^+ \mu^-$ for different values of ε_Z . The horizontal red (light red) band denotes the 1σ (3σ) allowed region from experiment [40]. The decay rate does not depend on ε .

The Z_D contribution to this rare decay is shown in Fig. 4. Since the decay rate depends only on the new axial-vector interaction of the dark Z , it is independent of ε . It is evident that ε_Z as large as 0.01 is allowed by the data at the 3σ confidence level (CL).

4.3 $B \rightarrow K^{(*)} \nu \bar{\nu}$

$B \rightarrow K^{(*)} \nu \bar{\nu}$ can be considered as a resonance decay with on-shell production of Z_D from B decay, followed by $Z_D \rightarrow \nu \bar{\nu}$. The decay widths for dark Z production can be written as [41]

$$\Gamma(B \rightarrow K Z_D) = \frac{|g_V^\nu|^2}{64\pi} \frac{\lambda_K^{3/2}}{m_B^3 M_{Z_D}^2} |f_+(M_{Z_D}^2)|^2, \quad (4.10)$$

$$\Gamma(B \rightarrow K^* Z_D) = \frac{\lambda_{K^*}^{1/2}}{16\pi m_B^3} (|H_0|^2 + |H_+|^2 + |H_-|^2), \quad (4.11)$$

where $\lambda_{K^{(*)}}$ stands for the Kallen function,

$$\lambda_{K^{(*)}}(q^2) = m_B^4 + m_{K^{(*)}}^4 + q^4 - 2(m_B^2 m_{K^{(*)}}^2 + m_{K^{(*)}}^2 q^2 + m_B^2 q^2), \quad (4.12)$$

and the helicity amplitudes are given by

$$\begin{aligned} H_0 &= g_A^\nu \left(-\frac{1}{2} (m_B + m_{K^*}) A_1(M_{Z_D}^2) x_{K^* Z_D} + \frac{m_{K^*} M_{Z_D}}{m_B + m_{K^*}} A_2(M_{Z_D}^2) (x_{K^* Z_D}^2 - 1) \right), \\ H_\pm &= \frac{g_A^\nu}{2} (m_B + m_{K^*}) A_1(M_{Z_D}^2) + g_V^\nu \frac{m_{K^*} M_{Z_D}}{m_B + m_{K^*}} V(M_{Z_D}^2) \sqrt{x_{K^* Z_D}^2 - 1}, \end{aligned} \quad (4.13)$$

with $x_{K^* Z_D} = (m_B^2 - m_{K^*}^2 - M_{Z_D}^2)/(2m_{K^*} M_{Z_D})$. The effective interaction strengths g_V^ν, g_A^ν are related to the loop functions by $g_{V(A)}^\nu = (E_L^{0,Z} \pm E_R^{0,Z})$. The form factors $V(q^2), A_1(q^2)$ and $A_2(q^2)$ can be found in Ref. [42].

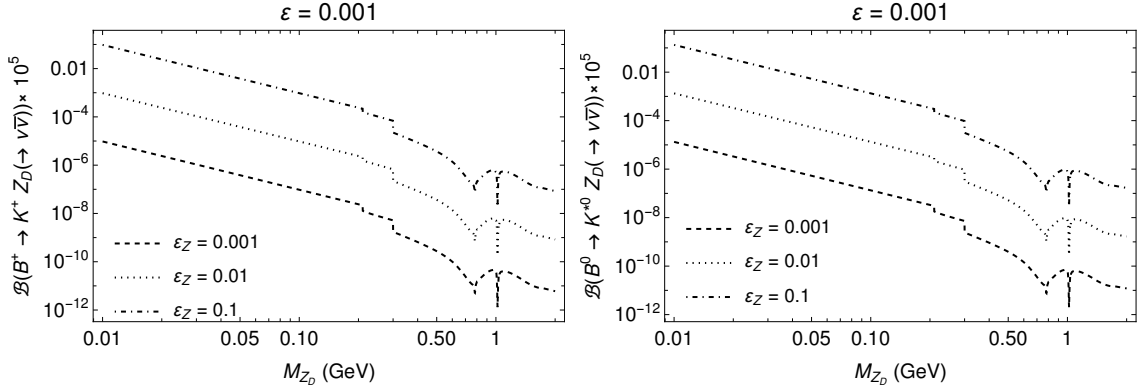


Figure 5. Branching fraction of $B \rightarrow K^{(*)}\nu\bar{\nu}$ as a function of the Z_D mass for three values of ε_Z and $\varepsilon = 0.001$.

The SM predictions for the above flavor changing decays are [43]

$$\mathcal{B}(B^+ \rightarrow K^+\nu\bar{\nu})_{SM} = (4.4 \pm 0.7) \times 10^{-6}, \quad (4.14)$$

$$\mathcal{B}(B^0 \rightarrow K^{*0}\nu\bar{\nu})_{SM} = (11.6 \pm 1.1) \times 10^{-6}. \quad (4.15)$$

A recent search for $B^+ \rightarrow K^+\nu\bar{\nu}$ by the Belle II experiment using a new inclusive tagging method led to the 90% CL upper bound [44],

$$\mathcal{B}(B^+ \rightarrow K^+\nu\bar{\nu}) < 4.1 \times 10^{-5}, \quad (4.16)$$

which, when combined with previous measurements by Belle and Babar puts the weighted average at

$$\mathcal{B}(B^+ \rightarrow K^+\nu\bar{\nu})_{WA} = (1.1 \pm 0.4) \times 10^{-5}. \quad (4.17)$$

Although the weighted average shows an enhancement over the SM expectation, caution should be exercised before treating it as a hint of new physics [43]. The most recent 90% CL upper bound on the branching fraction of $B \rightarrow K^*\nu\bar{\nu}$ is [45]

$$\mathcal{B}(B^0 \rightarrow K^{*0}\nu\bar{\nu}) < 1.8 \times 10^{-5}. \quad (4.18)$$

In Fig. 5, we plot the branching fractions for some benchmark values of ε_Z . We find that they are more than an order of magnitude smaller than the respective upper bounds even for ε_Z as large as 0.1.

4.4 Kaon decay and mixing

The flavor changing $K \rightarrow \pi\nu\bar{\nu}$ decay is mediated by the $s \rightarrow d\nu\bar{\nu}$ transition at the quark level. The two golden decay modes are $K^+ \rightarrow \pi^+\nu\bar{\nu}$ and $K_L \rightarrow \pi^0\nu\bar{\nu}$. The most recent measurement of the branching fraction of the charged kaon decay is that of the NA62 experiment [46],

$$\mathcal{B}(K^+ \rightarrow \pi^+\nu\bar{\nu}) = (10.6_{-3.4}^{+4.0}|_{stat} \pm 0.9_{sys}) \times 10^{-11}, \quad (4.19)$$

while the 90% CL upper bound on K_L decay from the KOTO experiment [47] is

$$\mathcal{B}(K_L \rightarrow \pi^0 \nu \bar{\nu}) < 4.9 \times 10^{-9}. \quad (4.20)$$

The SM expectations for these decays are [48, 49]

$$\mathcal{B}(K^+ \rightarrow \pi^+ \nu \bar{\nu})_{SM} = (8.4 \pm 1.0) \times 10^{-11}, \quad (4.21)$$

$$\mathcal{B}(K_L \rightarrow \pi^0 \nu \bar{\nu})_{SM} = (3.4 \pm 0.6) \times 10^{-11}. \quad (4.22)$$

The two decays are theoretically related in a model-independent manner by the Grossman-Nir bound [50] via $\mathcal{B}(K_L \rightarrow \pi^0 \nu \bar{\nu}) \lesssim 4.3 \mathcal{B}(K^+ \rightarrow \pi^+ \nu \bar{\nu})$.

As in the case of $B \rightarrow K \nu \nu$, the dark Z contribution to kaon decay can be considered to be resonant. The hadronic part of the amplitude is similar to that in Fig. 1 with s and d quarks in the external legs. The $s \rightarrow d Z_D$ transition is much suppressed compared to $b \rightarrow s Z_D$ and so the branching fractions of semileptonic kaon decays to invisible final states are tiny even for $\varepsilon_Z \sim 0.01$.

The neutral kaons K^0 and \bar{K}^0 undergo oscillations with a corresponding mass splitting just like the B_s^0 mesons. The leading SM contribution to the mass difference is given by

$$\Delta M_K^{SM} = \frac{G_F^2 M_K}{6\pi^2} M_W^2 (V_{cd} V_{cs}^*)^2 \eta_1 f_K^2 \hat{B}_K S_0(m_c^2/M_W^2), \quad (4.23)$$

where $\eta_1 = 1.38$ is the QCD correction factor, $f_K = 155.7(0.3)$ MeV [35] is the kaon decay constant, and $\hat{B}_K = 0.717(18)(16)$ [35] is the bag factor. The NP contribution is determined by the monopole operator and is given by

$$\Delta M_K^{NP} = \frac{1}{3} \frac{1}{M_K^2 - M_{Z_D}^2} f_K^2 \hat{B}_K M_K (E_{s,d}^{0,Z})_L^2 \left(1 - \frac{5}{8} \frac{m_s^2}{M_{Z_D}^2} \right). \quad (4.24)$$

The experimentally measured value is given by [37]

$$\Delta M_K = 3.484(6) \times 10^{-12} \text{ MeV}, \quad (4.25)$$

which is in accord with the SM expectation. We find that for $M_{Z_D} = 10$ MeV and $\varepsilon_Z = 0.001$, $\Delta M_K^{NP} = -4.64 \times 10^{-15}$ MeV which is consistent with measurement. Hence, ΔM_K does not impose a strong constraint on the model.

4.5 Radiative $K^+ \rightarrow \mu^+ \nu_\mu Z_D$ decays

The three body decay $K^+ \rightarrow \mu^+ \nu_\mu Z_D$ can be considered as a radiative correction to the standard $K^+ \rightarrow \mu^+ \nu_\mu$ decay in which Z_D is radiated off the muon leg and decays invisibly. Such dark emissions are likely when the dark boson mass is below $2m_\mu$ and is produced on shell.

For a general interaction of the dark boson with the muon,

$$\mathcal{L}_D^\mu = \bar{\mu}(g_V \gamma_\alpha + g_A \gamma_\alpha \gamma^5) \mu Z_D^\alpha, \quad (4.26)$$

the amplitude squared of the radiative decay process $K^+ \rightarrow \mu^+ \nu_\mu Z_D$ is

$$\begin{aligned}
\sum_{spins} |\mathcal{M}|^2 = & \frac{G_F^2 f_K^2 |V_{us}|^2}{(Q^2 - m_\mu^2)^2} \frac{1}{M_{Z_D}^2} (g_L^2 Q^4 (2E_\mu m_K (m_\mu^2 + M_{Z_D}^2 - Q^2) - 2E_D m_K M_{Z_D}^2 \\
& - m_K^2 m_\mu^2 + m_K^2 Q^2 - m_\mu^4 + m_\mu^2 Q^2 + 2M_{Z_D}^4 \\
& - m_\mu^2 M_{Z_D}^2 - M_{Z_D}^2 Q^2) + 6g_L g_R m_\mu^2 M_{Z_D}^2 Q^2 (Q^2 - m_K^2) \\
& + g_R^2 m_\mu^2 (-2E_\mu m_K^3 (m_\mu^2 + M_{Z_D}^2 - Q^2) \\
& + 2E_D (E_\nu M_{Z_D}^2 (m_K^2 - Q^2) + m_K^3 (Q^2 - m_\mu^2) \\
& + m_K Q^2 (m_\mu^2 + M_{Z_D}^2 - Q^2)) + M_K^4 m_\mu^2 + m_K^4 M_{Z_D}^2 \\
& - M_K^4 Q^2 + m_K^2 m_\mu^4 - m_K^2 m_\mu^2 Q^2 - 3m_K^2 M_{Z_D}^4 \\
& + 2m_K^2 m_\mu^2 M_{Z_D}^2 + M_{Z_D}^4 Q^2 - m_\mu^2 M_{Z_D}^2 Q^2) , \quad (4.27)
\end{aligned}$$

where $g_{L(R)} = g_V \mp g_A$. For a final state neutrino with energy E_ν and a muon with energy E_μ , $Q^2 = (k - q)^2 = m_K^2 - 2m_K E_\nu$ is the momentum transfer and E_D is the energy of the emitted dark boson. The three-body decay width is given by

$$\Gamma(K \rightarrow \mu \nu Z_D) = \frac{1}{64\pi^3 m_K} \int \sum_{spins} |\mathcal{M}|^2 dE_\mu dE_\nu , \quad (4.28)$$

with integration limits,

$$E_\mu^{min} = m_\mu , \quad E_\mu^{max} = \frac{m_K^2 + m_\mu^2 - M_{Z_D}^2}{2m_K} , \quad (4.29)$$

$$E_\nu^{min} = \frac{m_K^2 + m_\mu^2 - M_{Z_D}^2 - 2m_K E_\mu}{2(m_K - E_\mu + \sqrt{E_\mu^2 - m_\mu^2})} , \quad E_\nu^{max} = \frac{m_K^2 + m_\mu^2 - M_{Z_D}^2 - 2m_K E_\mu}{2(m_K - E_\mu - \sqrt{E_\mu^2 - m_\mu^2})} . \quad (4.30)$$

The emitted dark boson can subsequently decay to a pair of neutrinos and modify the missing energy spectrum of $K^+ \rightarrow \mu^+ \nu$. The NA62 experiment has set the following 90% CL upper limit from searches for kaon decays to single muon final states [51]:

$$\mathcal{B}(K^+ \rightarrow \mu^+ \nu \nu \bar{\nu}) < 1.0 \times 10^{-6} , \quad (4.31)$$

for a signal acceptance of $A_{\mu\nu\nu\nu} = 0.103$. We use this measurement to constrain the parameter space. However, since only a dark Z can decay to a pair of neutrinos, the bound does not apply to a dark photon. For Case A, the emission of the dark boson from the muon leg can occur with coupling $g_V = -e\varepsilon + \frac{g}{4c_W}\varepsilon_Z(-1 + 4s_W^2)$ and $g_A = -\frac{g}{4c_W}\varepsilon_Z$. The rate is mixing suppressed for this scenario and even for very light masses and $\varepsilon, \varepsilon_Z \sim 0.001$, the branching fraction stays well within the upper limit of Eq. (4.31), as shown in the left panel of Fig. 6. On the other hand, for Cases B and C, $g_V = -e\varepsilon + \frac{g}{4c_W}\varepsilon_Z(-1 + 4s_W^2) + g_D^\mu$. For small mixings, g_D^μ provides the dominant contribution and can be tightly constrained. From the right panel of Fig. 6, it can be seen that for Case B, g_D^μ must be less than 0.01 to satisfy Eq. (4.31).

The dark Z can also decay to $e^+ e^-$ instead of neutrinos. The rate for $K^+ \rightarrow \mu^+ \nu e^+ e^-$ has been calculated in the SM and measured in experiments. In the SM, this decay takes

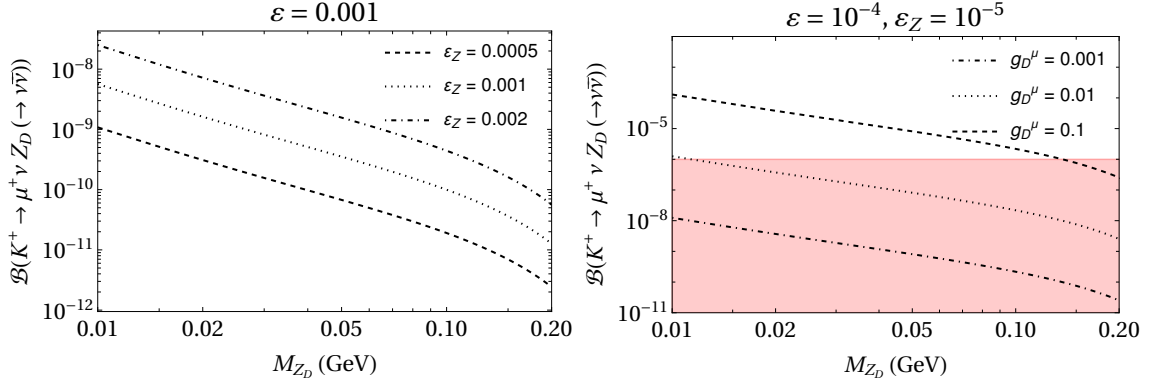


Figure 6. Dependence of the $K^+ \rightarrow \mu^+ + \text{invisible}$ branching fraction on the mixing parameters in Case A (left) and on the direct coupling g_D^μ in Case B (right). The red shaded region shows the 90% CL upper limit on the branching fraction in Eq. (4.31).

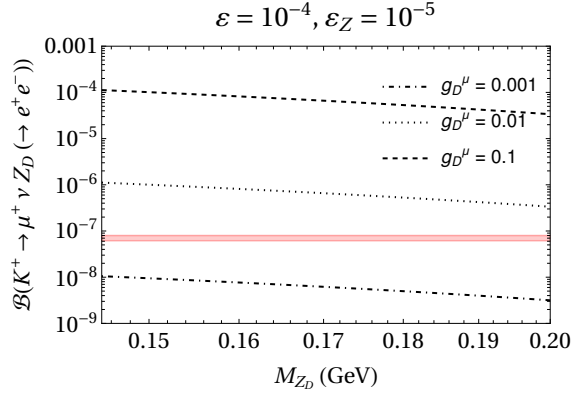


Figure 7. Dependence of the $K^+ \rightarrow \mu^+ \nu e^+ e^-$ branching fraction on g_D^μ in Case B. The red shaded region shows the 3σ interval of the branching fraction in Eq. (4.32).

place through the emission of a photon from the muon or the kaon (inner bremsstrahlung). The experimentally measured value of the branching fraction of $K^+ \rightarrow \mu^+ \nu_\mu e^+ e^-$ is [30, 52]

$$\mathcal{B}(K^+ \rightarrow \mu^+ \nu_\mu e^+ e^-) = (7.06 \pm 0.31) \times 10^{-8}, \quad (4.32)$$

for the invariant electron-positron mass $m_{ee} > 145$ MeV. In our model, this decay occurs via $K \rightarrow \mu \nu Z_D (\rightarrow e^+ e^-)$ and the above constraint applies for $M_{Z_D} > 145$ MeV. We find that $\varepsilon, \varepsilon_Z \sim 0.001$ is allowed by the data. For Case B, the dependence of the $K^+ \rightarrow \mu^+ \nu e^+ e^-$ branching fraction on g_D^μ is shown in Fig. 7. Clearly, $g_D^\mu \gtrsim 0.001$ produces an enhancement in the branching fraction for $145 < M_{Z_D} < 200$ MeV if $\varepsilon_Z < \varepsilon$ and Z_D decays primarily to $e^+ e^-$ below the muon threshold. This constraint does not apply for Case C as Z_D does not couple to electrons.

4.6 Radiative $\pi^+ \rightarrow \mu^+ \nu_\mu Z_D$ decays

Similar to radiative kaon decay, $\pi^+ \rightarrow \mu^+ \nu Z_D$ can be enhanced for $0 < M_{Z_D} < m_\pi - m_\mu$. The PIENU experiment has presented an upper bound on the ratio $R^{\pi\mu\nu X} = \Gamma(\pi^+ \rightarrow$

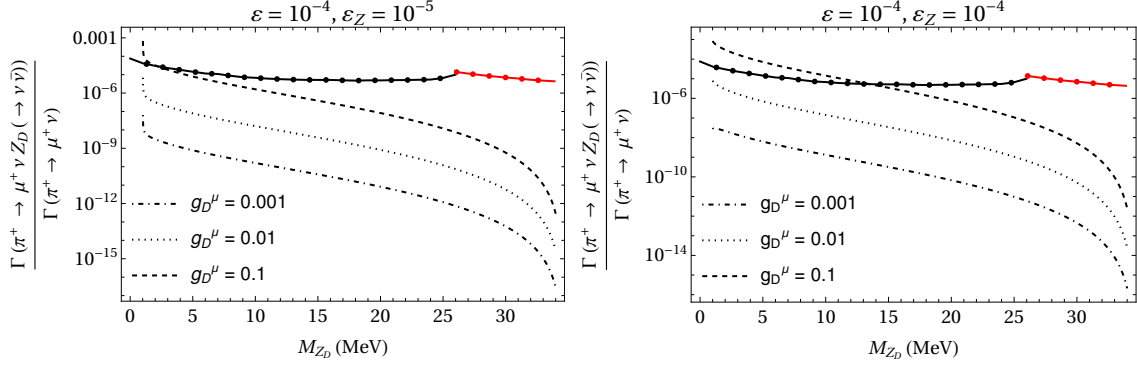


Figure 8. Dependence of $R^{\pi\mu\nu X} = \Gamma(\pi^+ \rightarrow \mu^+ \nu_\mu Z_D (\rightarrow \nu \bar{\nu})) / \Gamma(\pi^+ \rightarrow \mu^+ \nu_\mu)$ on g_D^μ for $\varepsilon_Z = 10^{-5}$ (left) and 10^{-4} (right). The black and red solid curves punctuated with points show the 90% CL upper limit from PIENU for the muon kinetic energy ranges, $T_\mu > 1.2$ MeV and $T_\mu < 1.2$ MeV, respectively.

$\mu^+ \nu_\mu X) / \Gamma(\pi^+ \rightarrow \mu^+ \nu_\mu)$ in the range $0 < M_X < 33.9$ MeV where X decays invisibly [53]. We utilize this bound to constrain our model parameters.

The decay rate is mixing suppressed in Case A and $\sim (g_D^\mu)^2$ for Cases B and C. For the general interaction in Eq. (4.26), the amplitude squared of $\pi^+ \rightarrow \mu^+ \nu_\mu Z_D$ is given by Eq. (4.27) with the substitutions $f_K \rightarrow f_\pi$, $V_{us} \rightarrow V_{ud}$ and $m_K \rightarrow m_\pi$. In Fig. 8, we show the dependence of $R^{\pi\mu\nu X}$ on g_D^μ . The 90% CL upper limit set by PIENU for the muon kinetic energy ranges, $T_\mu > 1.2$ MeV and $T_\mu < 1.2$ MeV, is shown by the solid black and red curves, respectively. We find that $g_D^\mu < 0.1$ is allowed for the $M_{Z_D} < 34$ MeV if the dark Z does not primarily decay to neutrinos i.e., if $\varepsilon_Z \ll \varepsilon$. However, if $\varepsilon_Z \gtrsim \varepsilon$, $\mathcal{B}(Z_D \rightarrow \nu \bar{\nu})$ is large (unity, if Z_D does not decay to electrons) and $g_D^\mu \geq 0.1$ is not allowed for $M_{Z_D} < 15$ MeV.

4.7 Atomic parity violation

Since the dark Z can couple to first generation SM fermions through mixing, the model parameters are subject to strong constraints from atomic parity violating observables. The interaction of the dark boson with the electromagnetic and weak currents of the SM in Eqs. (2.2) and (2.5) modify the weak charge Q_W of the proton and nuclei such as cesium (C_s), which are measured to be [49, 54, 55]

$$Q_W^{p,exp} = 0.0719(45), \quad Q_W^{^{133}C_s,exp} = -72.82(42). \quad (4.33)$$

The weak charges of the proton and $^{133}C_s$ nuclei are given by [56]

$$Q_W^{p,Z_D} = -2\rho_d g_{AV}^{ep} (\kappa_d \sin^2 \theta_W) \left(1 - \frac{\alpha}{2\pi}\right), \quad (4.34)$$

and

$$Q_W^{^{133}C_s,Z_D} = -2\rho_d [Z_{C_s} (g_{AV}^{ep} (\kappa_d \sin^2 \theta_W + 0.00005) + N_{C_s} (g_{AV}^{en} + 0.00006))] \left(1 - \frac{\alpha}{2\pi}\right), \quad (4.35)$$

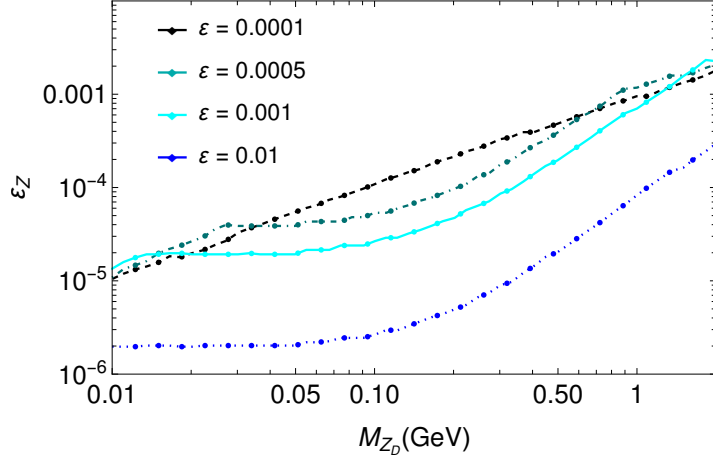


Figure 9. The 3σ CL upper bound on ε_Z from measurements of the proton and cesium weak charges in atomic parity violation experiments.

including radiative corrections. Here, $g_{AV}^{ep(en)}$ is the effective electron-proton (electron-neutron) coupling and is equal to $-1/2 + 2\sin^2\theta_W$ ($1/2$) in the SM at tree level. The Fermi constant G_F and the weak mixing angle θ_W are modified by the dark Z interaction to

$$G_F \rightarrow \rho_d G_F, \quad \sin^2\theta_W(Q^2) \rightarrow \kappa_d \sin^2\theta_W(Q^2), \quad (4.36)$$

where

$$\rho_d = 1 + \left(\frac{m_Z}{M_{Z_D}} \varepsilon_Z + \frac{M_{Z_D}}{m_Z} \varepsilon \tan\theta_W \right)^2 f \left(\frac{Q^2}{M_{Z_D}^2} \right), \quad (4.37)$$

and

$$\kappa_d = 1 - \varepsilon \left(\frac{m_Z}{M_{Z_D}} \varepsilon_Z + \frac{M_{Z_D}}{m_Z} \varepsilon \tan\theta_W \right) \frac{m_Z}{M_{Z_D}} \cot\theta_W f \left(\frac{Q^2}{M_{Z_D}^2} \right). \quad (4.38)$$

For the proton, $f(Q^2/M_{Z_D}^2) = M_{Z_D}^2/(Q^2 + M_{Z_D}^2)$ where Q^2 is the momentum transfer. For cesium, f is a constant that depends on M_{Z_D} . For example, $f \simeq 0.5$ for $M_{Z_D} \approx 2.4$ MeV while $f \simeq 1$ for $M_{Z_D} \approx 100$ MeV. We follow Ref. [56] to infer $f(Q^2/M_{Z_D}^2)$ for intermediate values of M_{Z_D} . The number of neutrons and protons in the cesium nucleus is $N_{C_s} = 78$ and $Z_{C_s} = 55$, respectively.

In Fig. 9, we plot the 3σ CL upper bound from APV on ε_Z for different values of ε . By and large, for larger values of ε , ε_Z is more constrained. Among the constraints discussed so far, APV places the strongest constraint on ε_Z in the few MeV-GeV mass range. The coupling g_D^μ which appears in Case B is unconstrained by APV. Again, because of our fine-tuned choice of g_D^e to cancel the Z_D coupling to electrons, Case C is also unconstrained by APV.

4.8 Neutrino trident and CE ν NS

Muon neutrinos can scatter off a nucleus and produce a pair of muons in a weak process known as neutrino trident production. The muon pair is produced through Z_D exchange

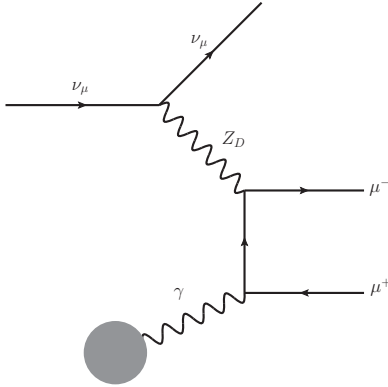


Figure 10. Neutrino trident mediated by Z_D .

as shown in Fig. 10. The neutrino trident has been measured in several neutrino beam experiments including CHARM-II [57] and CCFR [58]:

$$\frac{\sigma(\nu_\mu \rightarrow \nu_\mu \mu^+ \mu^-)_{\text{exp}}}{\sigma(\nu_\mu \rightarrow \nu_\mu \mu^+ \mu^-)_{\text{SM}}} = \begin{cases} 1.58 \pm 0.64 & (\text{CHARM-II}) \\ 0.82 \pm 0.28 & (\text{CCFR}). \end{cases} \quad (4.39)$$

Nonobservation of any excess puts strong upper limits on the couplings of Z_D with muons. In Ref. [59], bounds have been placed on the gauge coupling and mass of a Z' based on the $U(1)_{L_\mu-L_\tau}$ symmetry. For Cases B and C, we repurpose the bound in the $(M_{Z'}, g')$ plane to the (M_{Z_D}, ε_Z) plane by the scaling $(g')^2 \rightarrow g\varepsilon_Z g_D^\mu / 4c_W$, where the ε_Z suppression comes from the $Z_D \nu \nu$ vertex. Since the bound on g' was derived by assuming vector-like interactions of the lepton, it cannot be applied to Case A which has both vector and axial-vector interactions with the muon. However, we anticipate that a CCFR bound on Case A will not be as stringent as the APV bound.

The COHERENT experiment first observed coherent elastic neutrino-nucleus scattering (CE ν NS) in a CsI detector [60] and subsequently in a liquid Argon detector [61, 62]. The data have been used to set upper limits on gauged $U(1)_X$ model parameters [63–65]. In our model, CE ν NS can occur via the exchange of Z_D and so COHERENT data constrain ε_Z for a given Z_D mass. We rescale bound from Ref. [63] according to $g' \rightarrow \varepsilon_Z \frac{g}{c_W} g_V^\nu g_V^q$ with $g_V^\nu = 1/2$, $g_V^u = \frac{1}{2} - \frac{4}{3}s_W^2$, $g_V^d = -\frac{1}{2} + \frac{2}{3}s_W^2$. Bounds on ε_Z turn out to be much weaker than on a direct gauge coupling g' . For example, we find $\varepsilon_Z \lesssim 0.0005$ for $M_{Z_D} \lesssim 10$ MeV.

4.9 Collider and other bounds

It is possible for Z_D to be produced on- or off-shell from Z decay. An example is $Z \rightarrow \ell \ell Z_D$ where Z_D is radiated from one of the lepton legs. Z_D may then decay to a pair of leptons or jets, which lead to $Z \rightarrow 4\ell$ ($\ell = e, \mu$), final states that have been searched for at ATLAS [66, 67] and CMS [68, 69]. The results are consistent with the SM. The invariant 4ℓ mass peaks at the Z mass and places a bound for $M_{Z_D} \gtrsim 5$ GeV. For our model, the Z_D couplings to leptons are suppressed by the mixing parameters making the decay rate for $Z_D \rightarrow 4\ell$ small. Also, the emitted dark boson is expected to be soft and therefore will

not produce energetic leptons in the final state. Hence, the bounds from this decay do not impact our model. The same applies to NP searches in the jets + missing energy final state.

Recently, Belle II searched for an invisibly decaying Z' boson in $e^+e^- \rightarrow \mu^+\mu^- +$ missing energy channel [70]. The search puts an upper limit on the Z' coupling to muons to be between $0.05 - 1$ for $M_{Z'} < 6$ GeV under the assumption that Z' decays only to invisible particles. The bound becomes weaker for $\mathcal{B}(Z' \rightarrow \text{invisible}) < 1$. Consequently, this limit is not as competitive as the low energy bounds discussed previously.

The dark boson can contribute to the leptonic decay width of the W boson, which is measured very precisely. Additional contributions to $\Gamma(W \rightarrow \ell + \text{invisible})$ arising from $\Gamma(W \rightarrow \ell\nu Z_D, Z_D \rightarrow \nu\bar{\nu})$ can be significant due to the enhancement from the longitudinal polarization of the Z_D . In the limit $m_\ell, M_{Z_D} \ll M_W$, if Z_D decays mostly invisibly, the three body leptonic decay width is given by [14]

$$\Gamma(W \rightarrow \ell\nu Z_D) \simeq \frac{(C_{\ell\ell Z_D} - \tilde{C}_{\ell\ell Z_D})^2 G_F M_W^5}{512\sqrt{2}\pi^3 M_{Z_D}^2}, \quad (4.40)$$

where $C_{\ell\ell Z_D}, \tilde{C}_{\ell\ell Z_D}$ are the effective vector and axial-vector $Z_D\ell\ell$ couplings, respectively. For a dark photon, $C_{\ell\ell Z_D} = e\varepsilon$ and $\tilde{C}_{\ell\ell Z_D} = 0$, and for a dark Z , $C_{\ell\ell Z_D} = \frac{g}{\cos\theta_W}\varepsilon_Z g_V^\ell$ and $\tilde{C}_{\ell\ell Z_D} = \frac{g}{\cos\theta_W}\varepsilon_Z g_A^\ell$. The new contribution to the $W \rightarrow \ell + \text{invisible}$ decay is then given by

$$\Gamma(W \rightarrow \ell + \text{invisible}) = \Gamma(W \rightarrow \ell\nu Z_D) \cdot \mathcal{B}(Z_D \rightarrow \nu\bar{\nu}). \quad (4.41)$$

We conservatively require the new contribution to lie within the uncertainty of the measured decay width of the W boson. For Case A, if the dark boson mass is below the dimuon threshold, $\mathcal{B}(Z_D \rightarrow \nu\bar{\nu}) \sim 70\%$ for $\varepsilon_Z \sim \mathcal{O}(10^{-3})$. Then, since $\Gamma_W = 2.085 \pm 0.042$ GeV [49], the 2σ bound on the mixing parameters is given by

$$\varepsilon_Z \lesssim 0.08 \left(\frac{M_{Z_D}}{100 \text{ MeV}} \right), \quad (4.42)$$

which is not competitive with our previous bounds. The bound gets more restrictive if there is a direct coupling of the dark Z to muons, as we discuss later.

The LHCb collaboration has performed searches for dark photons in dimuon samples [71] and put stringent bounds on the mixing parameter. It is found that $\varepsilon \lesssim 10^{-4}$ for $M_{Z_D} \sim 200$ MeV and $\varepsilon \lesssim 0.0005$ for $M_{Z_D} \sim 2$ GeV at the 90% CL. This bound directly applies to Case A, and for Cases B and C, we recast the bound on ε to the coupling g_D^μ by appropriately scaling the effective $pp \rightarrow Z_D \rightarrow \mu\mu$ interaction strength from $(e\varepsilon)^2 \rightarrow (e\varepsilon)g_D^\mu$. This rules out $g_D^\mu > 10^{-3}$ for $M_{Z_D} > 210$ MeV.

5 Parameter fits

We fit the most recent experimental data for the exclusive decays, $B \rightarrow K^{(*)}\ell^+\ell^-$ and $B_s^0 \rightarrow \phi\mu^+\mu^-$, as well as the inclusive decays, $B \rightarrow X_s\ell^+\ell^-$, in different q^2 bins as listed in Table 1. Note that we only analyze data below the $c\bar{c}$ resonances. We use `flavio` [79]

Decay	Ref.	q^2 bin (GeV ²)	Measurement	SM expectation
$\frac{d\mathcal{B}}{dq^2}(B^0 \rightarrow K^{*0}\mu^+\mu^-) \times 10^8$	[72]	0.1 – 0.98	$11.06^{+0.67}_{-0.73} \pm 0.29 \pm 0.69$	10.60 ± 1.54
		1.1 – 2.5	$3.26^{+0.32}_{-0.31} \pm 0.10 \pm 0.22$	4.66 ± 0.74
		2.5 – 4.0	$3.34^{+0.31}_{-0.33} \pm 0.09 \pm 0.23$	4.49 ± 0.70
		4.0 – 6.0	$3.54^{+0.27}_{-0.26} \pm 0.09 \pm 0.24$	5.02 ± 0.75
$\frac{d\mathcal{B}}{dq^2}(B^+ \rightarrow K^{*+}\mu^+\mu^-) \times 10^8$	[73]	0.1 – 2.0	$5.92^{+1.44}_{-1.30} \pm 0.40$	7.97 ± 1.15
		2.0 – 4.0	$5.59^{+1.59}_{-1.44} \pm 0.38$	4.87 ± 0.76
		4.0 – 6.0	$2.49^{+1.10}_{-0.96} \pm 0.17$	5.43 ± 0.74
$\frac{d\mathcal{B}}{dq^2}(B^+ \rightarrow K^+\mu^+\mu^-) \times 10^8$	[73]	0.1 – 0.98	$3.32 \pm 0.18 \pm 0.17$	3.53 ± 0.64
		1.1 – 2.0	$2.33 \pm 0.15 \pm 0.12$	3.53 ± 0.58
		2.0 – 3.0	$2.82 \pm 0.16 \pm 0.14$	3.51 ± 0.52
		3.0 – 4.0	$2.54 \pm 0.15 \pm 0.13$	3.50 ± 0.63
		4.0 – 5.0	$2.21 \pm 0.14 \pm 0.11$	3.47 ± 0.60
$\frac{d\mathcal{B}}{dq^2}(B^0 \rightarrow K^0\mu^+\mu^-) \times 10^8$	[73]	0.1 – 2.0	$1.22^{+0.59}_{-0.52} \pm 0.06$	3.28 ± 0.52
		2.0 – 4.0	$1.87^{+0.55}_{-0.49} \pm 0.09$	3.25 ± 0.56
		4.0 – 6.0	$1.73^{+0.53}_{-0.48} \pm 0.09$	3.21 ± 0.54
$\frac{d\mathcal{B}}{dq^2}(B_s^0 \rightarrow \phi\mu^+\mu^-) \times 10^8$	[74]	0.1 – 0.98	$7.74 \pm 0.53 \pm 0.12 \pm 0.37$	11.31 ± 1.34
		1.1 – 2.5	$3.15 \pm 0.29 \pm 0.07 \pm 0.15$	5.44 ± 0.61
		2.5 – 4.0	$2.34 \pm 0.26 \pm 0.05 \pm 0.11$	5.14 ± 0.73
		4.0 – 6.0	$3.11 \pm 0.24 \pm 0.06 \pm 0.15$	5.50 ± 0.69
$\mathcal{B}(B^+ \rightarrow K^+e^+e^-) \times 10^8$	[75]	0.1 – 4.0	$18.0^{+3.3}_{-3.0} \pm 0.5$	13.73 ± 1.88
		4.0 – 8.12	$9.6^{+2.4}_{-2.2} \pm 0.3$	14.11 ± 1.88
$\mathcal{B}(B^0 \rightarrow K^{*0}e^+e^-) \times 10^7$	[76]	$0.03^2 - 1.0^2$	$3.1^{+0.9+0.2}_{-0.8-0.3} \pm 0.2$	2.56 ± 0.44
$\mathcal{B}(B \rightarrow X_s\mu^+\mu^-) \times 10^6$	[77]	1.0 – 6.0	$0.66^{+0.82+0.30}_{-0.76-0.24} \pm 0.07$	1.67 ± 0.15
$\mathcal{B}(B \rightarrow X_se^+e^-) \times 10^6$	[77]	1.0 – 6.0	$1.93^{+0.47+0.21}_{-0.45-0.16} \pm 0.18$	1.74 ± 0.16
$\frac{d\mathcal{B}}{dq^2}(B^+ \rightarrow K^+e^+e^-) \times 10^9$	[78]	1.1 – 6.0	$25.5^{+1.3}_{-1.2} \pm 1.1$	34.9 ± 6.2
$\frac{d\mathcal{B}}{dq^2}(B^0 \rightarrow K^{*0}e^+e^-) \times 10^9$	[78]	1.1 – 6.0	$33.3^{+2.7}_{-2.6} \pm 2.2$	47.7 ± 7.5

Table 1. Experimental measurements and SM expectations in q^2 bins. The SM χ^2 for the fit to all the observables is 93.56, and for just the muon modes it is 84.30.

to calculate the SM and NP expectations. We determine the allowed parameter values (denoted X) for each model using

$$\chi^2(X) = \sum_{i=1}^n \frac{(\mathcal{B}_i^{th}(X) - \mathcal{B}_i^{exp})^2}{\sigma_i^2}, \quad (5.1)$$

where n is the number of measurements, \mathcal{B}^{th} is the branching fraction, \mathcal{B}^{exp} is the corresponding experimental value and σ is the uncertainty from measurement and theory added in quadrature. For the theoretical uncertainty, we take the SM uncertainty estimated by `flavio`. To produce two-dimensional allowed regions, we marginalize over the third parameter and define the 1σ , 2σ and 3σ CL regions by $\chi^2 \leq \chi_{\min}^2 + 2.30$, $\chi^2 \leq \chi_{\min}^2 + 6.17$, and $\chi^2 \leq \chi_{\min}^2 + 11.83$, respectively, where χ_{\min}^2 is the global minimum. We define the pull with respect to the SM as $\sqrt{\chi_{SM}^2 - \chi^2}$.

For Cases A and B, we fit all 27 observables in Table 1, while for Case C, we exclude the 6 electron mode observables. $\chi_{SM}^2 = 93.56$ for the fit to muon and electron mode observables, and $\chi_{SM}^2 = 84.30$ for the fit to only muon mode observables.

5.1 Case A

In accordance with the bounds of the previous section, we restrict $\varepsilon \leq 0.001$ and $\varepsilon_Z \leq 0.002$. Our fit to the data shows an improvement with respect to the SM with $\chi_{NP}^2 = 85.8$ and pull = 2.79 at the best fit point,

$$M_{Z_D} = 10.07 \text{ MeV}, \quad \varepsilon = 1.6 \times 10^{-5}, \quad \varepsilon_Z = 0.002. \quad (5.2)$$

In Fig. 11, we show the marginalized 1σ (pink), 2σ (brown) and 3σ (dark brown) allowed regions in the (M_{Z_D}, ε_Z) and (M_{Z_D}, ε) planes. The best fit point is marked by a blue circle. Above $M_{Z_D} = 30$ MeV, Z_D contributes as a resonance to the $B^0 \rightarrow K^{*0} e^+ e^-$ branching fraction in the $[0.03^2, 1^2]$ GeV² bin, and we use the narrow width approximation to obtain the branching fraction. The sharp drop in the allowed values of ε_Z above 30 MeV is a consequence of this resonance. The bound relaxes gradually as the mass increases until about $M_{Z_D} \sim 300$ MeV when Z_D starts appearing as a narrow resonance in the 0.1 GeV² bin for $b \rightarrow s\mu\mu$, and causes another sharp drop in ε_Z . Similar drops in the allowed values of ε occur for the same reason. However, since the ε dependent $b \rightarrow s$ loop coefficient is suppressed compared to the q^2 independent, ε_Z dependent monopole contribution, the limits on ε are less stringent than those on ε_Z . The expected drop around $M_{Z_D} = 30$ MeV is not visible because we restrict the plot to $\varepsilon \leq 0.001$.

The model parameters are, however, in conflict with some low energy constraints. In particular, the weak charges measured in APV experiments rule out the entire allowed parameter space for $M_{Z_D} \lesssim 30$ MeV at more than 3σ . An important outcome of fitting the binned $b \rightarrow s\ell\ell$ data is that for $M_{Z_D} > 30$ MeV, we obtain upper limits on the mixing parameters that are even stronger than the APV limits.

Clearly, additional new physics is needed to reconcile all the data. To weaken the bound on ε_Z for $M_{Z_D} < 30$ MeV, we consider an additional contribution to the invisible decay width of the dark boson between 10% and 100% of the decay width to neutrinos. However, we find that this has a negligible impact on the fit. The best fit values of the mixing parameters remain the same with a slight improvement in the χ^2 .

5.2 Case B

The direct interaction of the dark Z with muons results in a contribution to the Wilson coefficient $\mathcal{C}_{9,\mu}$ apart from the mixing induced contribution in Eq. (2.10). The hadronic part of the amplitude is still loop induced and proportional to the mixing parameters. In our data analysis, we fix $\varepsilon = 10^{-4}$ and $\varepsilon_Z = 10^{-5}$ to evade stringent constraints from APV and meson mixing. We find the best fit point to be

$$M_{Z_D} = 10.3 \text{ MeV}, \quad g_D^\mu = 0.28, \quad (5.3)$$

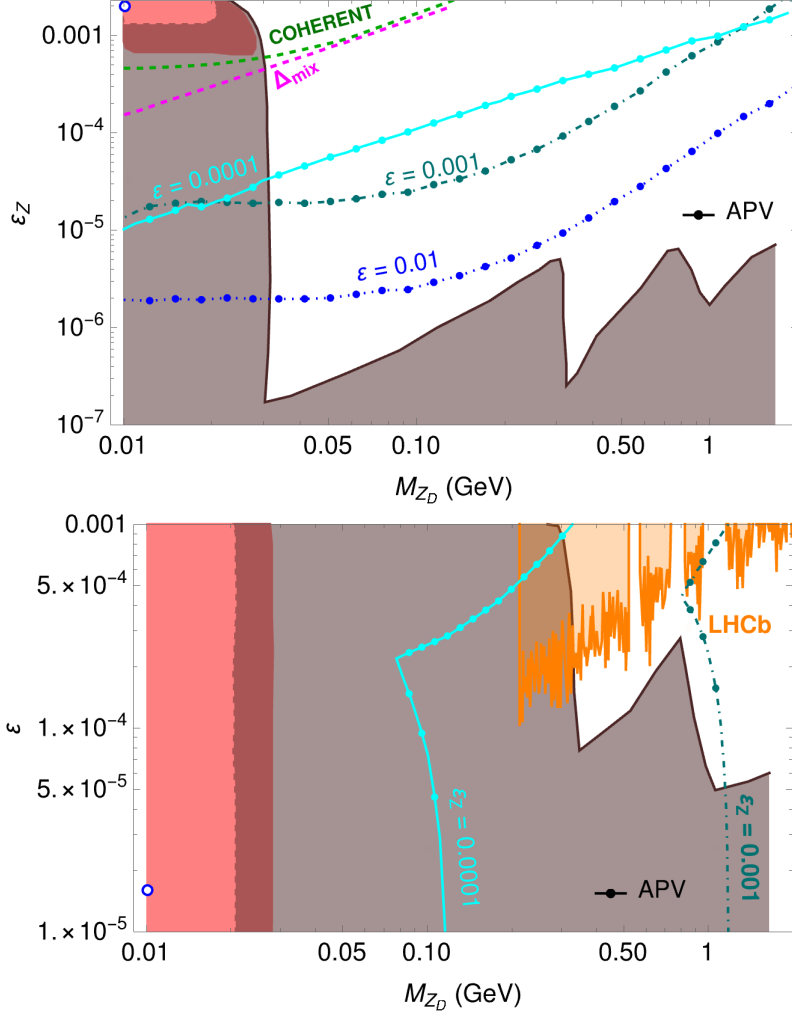


Figure 11. The 1σ (pink), 2σ (brown) and 3σ (dark brown) regions allowed by the data in Table 1 for Case A. The best fit point is marked by the blue circle. Top panel: 2σ upper limit from $B_s^0\text{-}\bar{B}_s^0$ mixing and 1σ upper limit from COHERENT neutrino scattering data are shown by the dashed magenta and green curves, respectively. The 3σ upper limits on ε_Z from the APV measurements for $\varepsilon = 0.0001, 0.001$ and 0.01 are shown by the cyan, dark cyan and blue dotted curves, respectively. Bottom panel: The orange shaded region is excluded by LHCb dark photon searches at the 90% CL. The 3σ upper limits on ε from APV measurements for $\varepsilon_Z = 0.0001$ and 0.001 are shown by the cyan and dark cyan curves, respectively; regions to the left of the curves are excluded.

with a $\chi_{NP}^2 = 75.15$ and pull = 4.29 from the SM. Case B represents a substantial improvement over Case A. Since there are only two fit parameters in this scenario, no marginalization is needed to obtain the allowed parameter space in Fig. 12.

Although we have chosen the mixing parameters to evade the APV bounds, due to the unsuppressed coupling of Z_D with muons, the $K^+ \rightarrow \mu^+ \nu X$ decay rate, where $X = \text{invisible}/e^+e^-$ rules out the entire parameter space in Fig. 12; see the right panel Fig. 6. (In Case A, this rate was suppressed by the mixing parameter.) The allowed parameter space is separately excluded by measurements of the W boson width because the $Z_D\mu\mu$

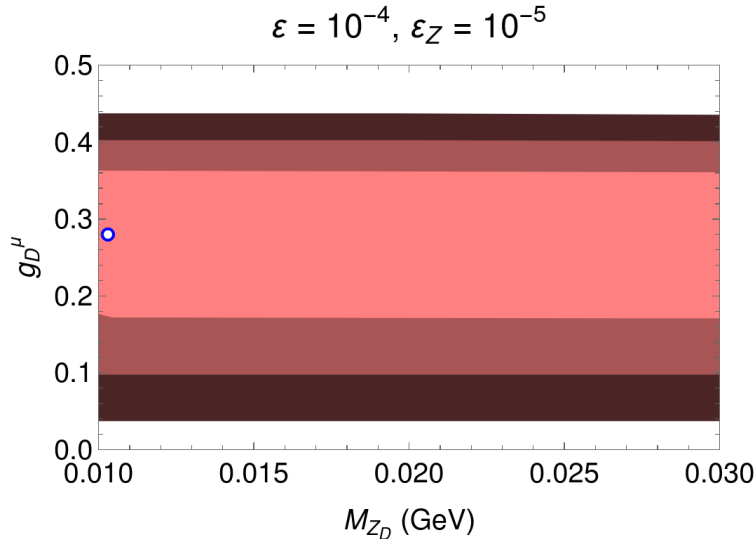


Figure 12. The 1σ , 2σ and 3σ allowed regions for Case B with the best fit point marked by a blue circle. However, the entire parameter space is ruled out by measurements of $K^+ \rightarrow \mu^+ \nu X$, $X = \text{invisible}/e^+e^-$) and separately by the W boson width.

interaction contributes to $\Gamma(W \rightarrow \mu\nu Z_D)$. As in Section 4.9, we require $\Gamma_W = 2.085 \pm 0.042$ GeV [49], and obtain the 2σ bound,

$$g_D^\mu < 0.022 \left(\frac{M_{Z_D}}{100 \text{ MeV}} \right), \quad (5.4)$$

which is in agreement with Ref. [14]. We do not show these constraints in Fig. 12 since the entire region is ruled out.

As a further extension of Case B, consider an additional axial-vector coupling of the dark Z to muons:

$$\mathcal{L}_D^Z \supset g_D^\mu \bar{\mu} \gamma_\nu \mu Z_D^\nu + g_{DA}^\mu \bar{\mu} \gamma_\nu \gamma_5 \mu Z_D^\nu. \quad (5.5)$$

The axial-vector interaction generates a new contribution to the Wilson coefficient $\mathcal{C}_{10,\mu}$. Introduction of an additional parameter improves the quality of the fit and results in $g_{DA}^\mu \sim -g_D^\mu$ which is in accordance with global fits for the scenario, $\mathcal{C}_9 = -\mathcal{C}_{10}$. However, due to additional contributions to the branching fractions of leptonic kaon decays, leptonic W decay, and $\mathcal{B}(B_s \rightarrow \mu\mu)$, we anticipate even more stringent constraints on the parameter space than before. Hence, we do not entertain this possibility any further.

5.3 Case C

In addition to g_D^μ , we now consider a direct coupling g_D^e of Z_D to electrons. As mentioned earlier, we assume that g_D^e is fine-tuned to cancel the Z_D coupling to electrons via mixing. Then, all observables for the electron mode are well described by the SM. The motivation for this scenario is that it provides an alternate way to bypass the APV constraints and relax bounds on the mixing parameters. We redo the fit to the $b \rightarrow s$ data except the 6 electron mode observables in Table 1. This reduces the number of $b \rightarrow s$ observables from

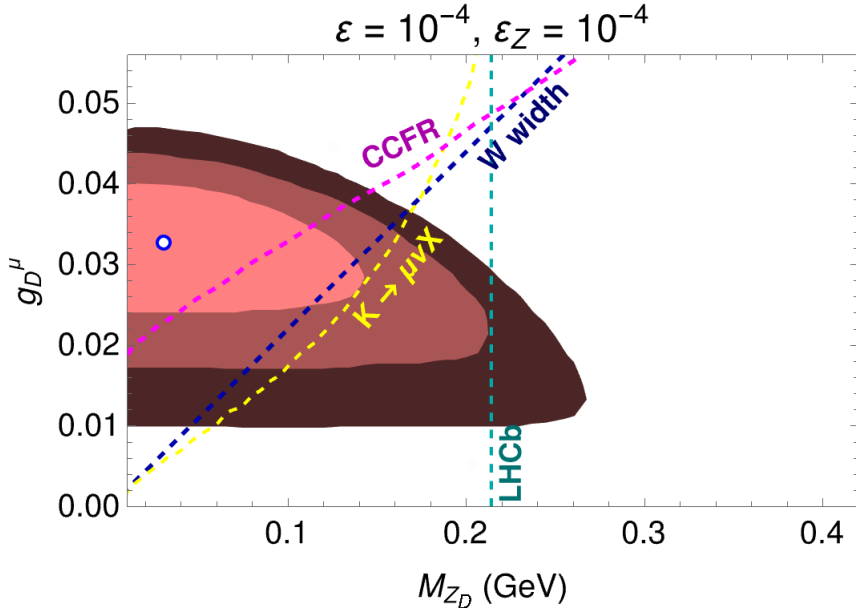


Figure 13. The 1σ , 2σ and 3σ allowed regions for Case C with the best fit point marked by a blue circle. Upper limits from neutrino trident production at CCFR (at 95% CL), $K \rightarrow \mu\nu X$ (at 90% CL) and the W width (at 95% CL) are shown by the dashed magenta, yellow and dark blue curves, respectively. Dark photon searches at LHCb rule out the region to the right of the vertical dashed dark cyan line at 90% CL.

27 to 21. We set $\epsilon = \epsilon_Z = 10^{-4}$ to satisfy bounds from $B_s^0 - \bar{B}_s^0$ mixing. The best fit point is

$$M_{Z_D} = 30.2 \text{ MeV}, \quad g_D^\mu = 0.033, \quad (5.6)$$

with $\chi_{NP}^2 = 56.90$ and pull = 5.23 ($\chi_{SM}^2 = 84.30$). This is a marked improvement over the previous cases. As expected, g_D^μ is an order of magnitude smaller than in Case B since ϵ_Z is larger by an order of magnitude. The allowed region with exclusions from all applicable bounds is shown in Fig. 13. The most stringent constraints are provided by neutrino trident production at CCFR (dashed magenta, 95% CL), $K \rightarrow \mu + \text{invisible}$ (dashed yellow, 90% CL) and the W width (dashed dark blue, 95% CL). Dark photon searches at LHCb rule out the region to the right of the vertical dashed dark cyan line at 90% CL. A region of parameter space bordered by $100 \lesssim M_{Z_D} \lesssim 200$ MeV and $0.015 \lesssim g_D^\mu \lesssim 0.035$ explains the binned $b \rightarrow s\mu^+\mu^-$ data at 2σ CL and is consistent with other bounds.

6 Muon anomalous magnetic moment

Measurements of the anomalous magnetic moment of the muon $a_\mu = (g - 2)_\mu/2$ [80, 81] differ from the SM expectation [82] by

$$\Delta a_\mu = a_\mu^{exp} - a_\mu^{SM} = 251(59) \times 10^{-11}. \quad (6.1)$$

In Case A, Z_D couples to muons via mixing, while in Cases B and C, Z_D couples directly to muons. The new contribution to a_μ in the three cases is given by [83]

$$a_\mu^A = \frac{m_\mu^2}{4\pi^2} \int_0^1 \frac{dx}{m_\mu^2 x^2 + M_{Z_D}^2 (1-x)} \left[(e\varepsilon)^2 x^2 (1-x) + \left(\frac{g(-1 + 4s_W^2)}{4c_W} \varepsilon_Z \right)^2 x^2 (1-x) + \left(\frac{g}{4c_W} \varepsilon_Z \right)^2 (x(1-x)(x-4) - 2x^3 m_\mu^2 / M_{Z_D}^2) \right], \quad (6.2)$$

$$a_\mu^{B,C} = \frac{(g_D^\mu m_\mu)^2}{4\pi^2} \int_0^1 \frac{x^2 (1-x)}{m_\mu^2 x^2 + M_{Z_D}^2 (1-x)} dx. \quad (6.3)$$

The FCNC constrained values of g_D^μ yield values of a_μ much larger than dictated by Eq. (6.1). Also, the axial-vector contribution to a_μ in Case A leads to an overall enhancement in the total yield of a_μ . For the best-fit points, we find $a_\mu^A = -3.45 \times 10^{-7}$, $a_\mu^B = 0.00077$ and $a_\mu^C = 7.38 \times 10^{-6}$. This suggests that some other source of new physics is needed to suppress the contribution. One possibility is a dark charged scalar which gives a negative contribution to a_μ .

7 Summary

We performed a comprehensive study of the contributions of a dark photon and dark Z to $b \rightarrow s\ell^+\ell^-$ observables. We correctly treated the FCNC decay amplitudes via the monopole and dipole operators of the dark bosons, and included the decay of the dark boson to light hadronic states to calculate its width. We implemented a fit to the binned $b \rightarrow s\ell^+\ell^-$ data to find the preferred values of the mass and mixing parameters.

We find that the base model with no direct Z_D couplings to charged leptons is ruled out by constraints from low energy experiments. Two extensions of the model with direct muon and electron couplings provide an improvement in the fit to $b \rightarrow s$ data over both the SM and base model without direct couplings. However, the many constraints permit only one of the extensions, with the viable parameter space confined to a small region. Consistency with measurements of the anomalous magnetic moment of the muon requires yet another source of new physics. We summarize the main results for each case below.

- **Case A:** For the base Z_D model, we find that $\varepsilon_Z \sim 10^{-3}$ and $M_{Z_D} \lesssim 30$ MeV is required to explain the binned $b \rightarrow s\ell\ell$ branching fraction data; see Fig. 11. However, the parameter space is excluded primarily by measurements of the proton and cesium weak charges in atomic parity violation experiments. Above $M_{Z_D} = 30$ MeV, the mixing parameters are severely constrained by FCNC measurements to which Z_D contributes as a sharp resonance.
- **Case B:** Case A is extended with a direct coupling of Z_D with muons. To respect bounds on ε and ε_Z from meson mixing and APV, we fix $\varepsilon = 10^{-4}$ and $\varepsilon_Z = 10^{-5}$. As a result, the parameter space is restricted to $M_{Z_D} < 30$ MeV. The coupling $g_D^\mu \gtrsim 0.1$ provides an unsuppressed contribution to the branching fraction to the muon modes. The entire parameter space is ruled out because of enhancements to $K \rightarrow \mu\nu X$ and to the W boson width.

- **Case C:** In addition to a direct muon coupling, Z_D has a fine-tuned direct coupling to electrons to cancel its coupling to electrons through mixing. This avoids the constraints from APV and $K \rightarrow \mu\nu e^+ e^-$. A fit to the $b \rightarrow s\mu^+\mu^-$ observables gives a best fit at $M_{Z_D} = 30.2$ MeV and $g_D^\mu = 0.033$ for $\varepsilon = \varepsilon_Z = 10^{-4}$ with a pull of 4.94 from the SM. Bounds from neutrino trident production at CCFR, LHCb dark photon searches, W width measurements and $K \rightarrow \mu\nu X$ rule out much of the allowed parameter space as shown in Fig. 13. A 2σ region around $100 \lesssim M_{Z_D} \lesssim 200$ MeV and $0.015 \lesssim g_D^\mu \lesssim 0.03$ remains viable provided a fine-tuned cancellation with other new physics is arranged to satisfy the constraint from the a_μ measurement.

Acknowledgments: We thank W. Altmannshofer and J. Dror for useful discussions, and J. Kumar for technical help on `flavio`. A.R. acknowledges the hospitality of the Department of Physics, University of Basel where his visit was supported through the SU-FPDC Grant Program. A.D. and L.M. are supported in part by the U.S. National Science Foundation under Grant No. PHY-1915142. D.M. is supported in part by the U.S. Department of Energy under Grant No. de-sc0010504.

A Form factors

The form factors (FFs) for transitions to the vector hadronic states, $B \rightarrow K^*$, $B \rightarrow \rho$, $B \rightarrow \omega$, $B_s \rightarrow \phi$, $B_s \rightarrow K^*$ are as below. The vector and tensor hadronic currents are parameterized by seven FFs [84]:

$$\begin{aligned} c_V \langle K^*(p, \eta) | \bar{s} \gamma^\mu (1 \mp \gamma_5) b | \bar{B}(p_B) \rangle &= P_1^\mu \mathcal{V}_1(q^2) \pm P_2^\mu \mathcal{V}_2(q^2) \pm P_3^\mu \mathcal{V}_3(q^2) \pm P_P^\mu \mathcal{V}_P(q^2), \\ c_V \langle K^*(p, \eta) | \bar{s} i q_\nu \sigma^{\mu\nu} (1 \pm \gamma_5) b | \bar{B}(p_B) \rangle &= P_1^\mu T_1(q^2) \pm P_2^\mu T_2(q^2) \pm P_3^\mu T_3(q^2), \end{aligned} \quad (\text{A.1})$$

where the Lorentz structures P_i^μ are defined by [85]

$$\begin{aligned} P_1^\mu &= 2\varepsilon^\mu_{\alpha\beta\gamma} \eta^{*\alpha} p^\beta q^\gamma, & P_2^\mu &= i\{(m_B^2 - m_{K^*}^2)\eta^{*\mu} - (\eta^* \cdot q)(p + p_B)^\mu\}, \\ P_3^\mu &= i(\eta^* \cdot q)\{q^\mu - \frac{q^2}{m_B^2 - m_{K^*}^2}(p + p_B)^\mu\}, & P_P^\mu &= i(\eta^* \cdot q)q^\mu, \end{aligned} \quad (\text{A.2})$$

where η is the vector meson polarization and $\varepsilon_{0123} = +1$ defines the convention for the Levi-Civita tensor. The factor c_V accounts for the flavor content of particles: $c_V = \sqrt{2}$ for ρ^0 , ω and $c_V = 1$ otherwise.² The parameterization in Eq. (A.1) makes the correspondence between vector and tensor FFs explicit. The correspondence between $\mathcal{V}_{P,1,2,3}$ and the more traditional FFs $A_{0,1,2,3}$ and V is as follows:

$$\begin{aligned} \mathcal{V}_P(q^2) &= -\frac{2m_{K^*}}{q^2} A_0(q^2), & \mathcal{V}_1(q^2) &= -\frac{V(q^2)}{m_B + m_{K^*}}, & \mathcal{V}_2(q^2) &= -\frac{A_1(q^2)}{m_B - m_{K^*}}, \\ \mathcal{V}_3(q^2) &= \frac{m_B + m_{K^*}}{q^2} A_1(q^2) - \frac{m_B - m_{K^*}}{q^2} A_2(q^2) \equiv \frac{2m_{K^*}}{q^2} A_3(q^2). \end{aligned} \quad (\text{A.3})$$

²To be precise, c_V is $\sqrt{2}$ for ρ^0 in $b \rightarrow u$ and for ω , and $-\sqrt{2}$ for ρ^0 in $b \rightarrow d$, with the flavor wave functions $\rho^0 \sim (\bar{u}u - \bar{d}d)/\sqrt{2}$ and $\omega \sim (\bar{u}u + \bar{d}d)/\sqrt{2}$. We assume that ϕ is a pure $s\bar{s}$ state.

The form factors f_+^P , f_0^P and f_T^P which are relevant for the $B \rightarrow P$ transition, where P denotes the pseudoscalar hadronic states π , K or η , are defined as follows [86]:³

$$\begin{aligned}\langle P(p)|V_\mu^P|B(p_B)\rangle &= \{(p+p_B)_\mu - \frac{m_B^2 - m_P^2}{q^2} q_\mu\} f_+^P(q^2) + \{\frac{m_B^2 - m_P^2}{q^2} q_\mu\} f_0^P(q^2), \\ \langle P(p)|J_\mu^{P,\sigma}|B(p_B)\rangle &= \frac{i}{m_B + m_P} \{q^2(p+p_B)_\mu - (m_B^2 - m_P^2)q_\mu\} f_T^P(q^2, \mu),\end{aligned}\quad (\text{A.4})$$

where $V_\mu^{\pi,\eta} = \bar{u}\gamma_\mu b$ is the standard weak current, V_μ^K is given by $V_\mu^K = \bar{s}\gamma_\mu b$ and $J_\mu^{\pi(\eta),\sigma} = \bar{d}\sigma_{\mu\nu}q^\nu b$, $J_\mu^{K,\sigma} = \bar{s}\sigma_{\mu\nu}q^\nu b$ are penguin currents. The momentum transfer is given by $q = p_B - p$ and the physical range in q^2 is $0 \leq q^2 \leq (m_B - m_P)^2$.

The hadronic current in the decay process $K^+ \rightarrow \pi^+ \nu \bar{\nu}$ is given by [87]

$$\langle \pi^+(p_\pi) | \bar{d}\gamma^\mu (1 \mp \gamma_5) s | K^+(p_K) \rangle = f_+(q^2)(p_K + p_\pi)^\mu + f_-(q^2)(p_K - p_\pi)^\mu, \quad (\text{A.5})$$

where $q^2 = (p_K - p_\pi)^2$ and $f_\pm(q^2)$ are the FFs [88, 89],

$$f_\pm(q^2) = f_\pm(0)(1 + \lambda_\pm(q^2/m_{\pi^+}^2)), \quad (\text{A.6})$$

with $\lambda_- = 0$, $f_-(0) = -0.332$, $f_+(0) = 0.57$ [88] and

$$\lambda_+(q^2/m_{\pi^+}^2) = \frac{1}{m_\pi^2} \sqrt{(m_K^2 + m_\pi^2 - q^2)^2 - 4m_K^2 m_\pi^2}. \quad (\text{A.7})$$

The three different components to the decay processes $K_L^0 \rightarrow \pi^0 e^+ e^-$ and $K_L^0 \rightarrow \pi^0 \nu \bar{\nu}$ are: 1) a CP-conserving process which proceeds through two-photon exchanges, 2) an indirect CP-violating effect proportional to the parameter ε , and 3) the direct CP-violating effect which is manifested in the penguin reactions. We consider the the contribution of the direct CP-violating effect to constrain the mixing parameters (ε , ε_Z). Note that the amplitude is proportional to the imaginary components of the CKM matrix elements in the hadronic loop coefficients in Appendix B. The form factors that describe the direct CP-violating contribution, which is manifested in the penguin reactions, to the hadronic current $K_L^0 \rightarrow \pi^0$ can be found in [90]

$$\begin{aligned}\langle \pi^0(K) | \bar{s}\gamma^\mu d | K_L^0(P) \rangle &= \left((P+K)^\mu f_+^{K^0\pi^0}(z) + (P-K)^\mu f_-^{K^0\pi^0}(z) \right), \quad (\text{A.8}) \\ f_-^{K^0\pi^0}(z) &= \frac{1-r_\pi^2}{z} \left(f_0^{K^0\pi^0}(z) - f_+^{K^0\pi^0}(z) \right),\end{aligned}$$

where $r_\pi = M_\pi/M_K$, $z = q^2/M_{K^0}^2$. The slopes extracted from $K_{\ell 3}$ decays by neglecting isospin breaking are [30, 91–94],

$$f_{0,+}(z) \equiv f_{0,+}^{K^0\pi^0}(z) = \frac{f_+(0)}{1 - \lambda_{0,+} z}, \quad \lambda_0 = 0.18, \quad \lambda_+ = 0.32, \quad (\text{A.9})$$

in the pole parametrization. Accounting for isospin breaking in $\pi^0 - \eta$ mixing, at zero momentum transfer one finds [95],

$$f_+(0) = (1.0231)^{-1} f_+^{K^0\pi^+}(0) \approx 0.939, \quad (\text{A.10})$$

³The following notation is frequently used in the literature: $f_+ = F_1$ and $f_0 = F_0$.

with the Leutwyler-Ross prediction $f_+^{K^0\pi^+}(0) = 0.961(8)$ [96], which is confirmed by lattice studies [97–99].

The hadronic current $K_S^0 \rightarrow \pi^0$ is given by [100]

$$\langle \pi^0(K) | \bar{s}\gamma^\mu d | K_S^0(P) \rangle = W_S(Z) (P + K)^\mu, \quad (\text{A.11})$$

where

$$W_S(Z) = (a_S + b_S Z), \quad (\text{A.12})$$

with $|a_S| = 1.08_{-0.21}^{+0.26}$, $b_S/a_S = m_{K_S}^2/m_\rho^2$, and $z = q^2/m_{K_S}^2$.

B Hadronic loop contributions

The Wilson coefficients for the dark photon contributions in Eq. (2.8) for $b \rightarrow sZ_D$ are obtained using the Peng4BSM@LO package [21]:

$$(E_{c2,c3}^{0,A})_L = 0, \quad (\text{B.1})$$

$$(E_{c2,c3}^{0,A})_R = 0, \quad (\text{B.2})$$

$$\begin{aligned} (E_{c2,c3}^{2,A})_L = & \sum_{j=2}^3 \frac{e^3 \varepsilon (V_{\text{CKM}}^{j2})^* V_{\text{CKM}}^{j3} \delta_{c2 c3}}{1152 \pi^2 (x_1^2 - 1)^4 (x_j^2 - 1)^4 M_W^2 s_w^2} \\ & (4 (3x_1^8 - 30x_1^6 + 54x_1^4 - 32x_1^2 + 8) (x_j^2 - 1)^4 \log(x_1) - \\ & (x_1^2 - 1) (4 (x_1^2 - 1)^3 (3x_j^8 - 30x_j^6 + 54x_j^4 - 32x_j^2 + 8) \log(x_j) + \\ & (x_j^2 - 1) (25x_j^4 - 19x_j^6 + x_1^6 (32x_j^4 - 57x_j^2 + 19) + \\ & (-32x_j^6 + 75x_j^2 - 25) x_1^4 + (57x_j^6 - 75x_j^4) x_1^2)) , \end{aligned} \quad (\text{B.3})$$

$$(E_{c2,c3}^{2,A})_R = 0, \quad (\text{B.4})$$

$$\begin{aligned} (M_{c2,c3}^{1,A})_L = & \sum_{j=2}^3 - \frac{ie^3 m_s \varepsilon (V_{\text{CKM}}^{j2})^* V_{\text{CKM}}^{j3} \delta_{c2 c3}}{384 \pi^2 (x_1^2 - 1)^4 (x_j^2 - 1)^4 M_W^2 s_w^2} \\ & (-12x_1^4 (3x_1^2 - 2) (x_j^2 - 1)^4 \log(x_1) + \\ & (x_1^2 - 1) (12 (x_1^2 - 1)^3 x_j^4 (3x_j^2 - 2) \log(x_j) + \\ & (x_j^2 - 1) (x_1^6 (-29x_j^4 + 31x_j^2 - 8) + x_j^2 (8x_j^4 + 5x_j^2 - 7) + \\ & (29x_j^6 - 6x_j^2 - 5) x_1^4 + (-31x_j^6 + 6x_j^4 + 7) x_1^2)) , \end{aligned} \quad (\text{B.5})$$

$$\begin{aligned}
(M_{c2,c3}^{1,A})_R &= \sum_{j=2}^3 \frac{ie^3 m_b \varepsilon (V_{\text{CKM}}^{j2})^* V_{\text{CKM}}^{j3} \delta_{c2 c3}}{384\pi^2 (x_1^2 - 1)^4 (x_j^2 - 1)^4 M_W^2 s_w^2} \\
&\quad (-12x_1^4 (3x_1^2 - 2) (x_j^2 - 1)^4 \log(x_1) + \\
&\quad (x_1^2 - 1) (12 (x_1^2 - 1)^3 x_j^4 (3x_j^2 - 2) \log(x_j) + \\
&\quad (x_j^2 - 1) (x_1^6 (-29x_j^4 + 31x_j^2 - 8) + x_j^2 (8x_j^4 + 5x_j^2 - 7) + \\
&\quad (29x_j^6 - 6x_j^2 - 5) x_1^4 + (-31x_j^6 + 6x_j^4 + 7) x_1^2)) . \tag{B.6}
\end{aligned}$$

The equations are simplified by using CKM matrix unitarity and introducing $x_j = m_j/M_W$ where m_j are the masses of the internal quarks in the loop and $\delta_{c2 c3}$ is the Kronecker delta function on the color states of the incoming and outgoing quarks.

The Wilson coefficients for the dark Z contributions in Eq. (2.8) for $b \rightarrow sZ_D$ are

$$\begin{aligned}
(E_{c2,c3}^{0,Z})_L &= \sum_{j=2}^3 \frac{e^3 \varepsilon_Z (V_{\text{CKM}}^{j2})^* V_{\text{CKM}}^{j3} \delta_{c2 c3}}{64\pi^2 (x_1^2 - 1)^2 (x_j^2 - 1)^2 c_w s_w^3} \\
&\quad (2x_1^2 (3x_1^2 + 2) (x_j^2 - 1)^2 \log(x_1) + \\
&\quad (x_1^2 - 1) (-2 (x_1^2 - 1) x_j^2 (3x_j^2 + 2) \log(x_j) + \\
&\quad (x_j^2 - 1) ((x_j^2 - 1) x_1^4 - (x_j^4 - 6) x_1^2 + x_j^2 (x_j^2 - 6)))) , \tag{B.7}
\end{aligned}$$

$$(E_{c2,c3}^{0,Z})_R = 0 , \tag{B.8}$$

$$\begin{aligned}
(E_{c2,c3}^{2,Z})_L &= \sum_{j=2}^3 \frac{e^3 \varepsilon_Z (V_{\text{CKM}}^{j2})^* V_{\text{CKM}}^{j3} \delta_{c2 c3}}{2304\pi^2 (x_1^2 - 1)^4 (x_j^2 - 1)^4 c_w M_W^2 s_w^3} \\
&\quad (4 \log(x_1) ((3x_1^8 - 36x_1^6 + 36x_1^4 - 64x_1^2 + 16) s_w^2 - 3 (4 - 12x_1^2 + \\
&\quad x_1^8 (1 - s_w^2) - 8x_1^6 (1 - s_w^2) + 3x_1^4 (8 (1 - s_w^2) + 3))) \\
&\quad (x_j^2 - 1)^4 - (x_1^2 - 1) (4 (x_1^2 - 1)^3 \log(x_j) \\
&\quad ((3x_j^8 - 36x_j^6 + 36x_j^4 - 64x_j^2 + 16) s_w^2 - 3 (4 - 12x_j^2 + \\
&\quad x_j^8 (1 - s_w^2) - 8x_j^6 (1 - s_w^2) + 3x_j^4 (8 (1 - s_w^2) + 3))) - \\
&\quad (x_1^2 - x_j^2)(x_j^2 - 1) (10 - 5x_1^2 - 11x_1^4 - 5x_j^2 - 26x_1^2 x_j^2 + \\
&\quad 43x_1^4 x_j^2 - 11x_j^4 + 43x_1^2 x_j^4 - 38x_1^4 x_j^4 + \\
&\quad (1 - s_w^2) (-58 - 73x_j^2 + 29x_j^4 + x_1^2 (-145x_j^4 + 422x_j^2 - 73) + \\
&\quad x_1^4 (14x_j^4 - 145x_j^2 + 29)) - s_w^2 (58 + 23x_j^2 + 9x_j^4 + \\
&\quad (50x_j^4 + 31x_j^2 + 9) x_1^4 + (31x_j^4 - 234x_j^2 + 23) x_1^2)) , \tag{B.9}
\end{aligned}$$

$$(E_{c2,c3}^{2,Z})_R = 0 , \tag{B.10}$$

$$\begin{aligned}
(M_{c_2, c_3}^{1, Z})_L = & \sum_{j=2}^3 \frac{ie^3 m_s \varepsilon_Z (V_{\text{CKM}}^{j2})^* V_{\text{CKM}}^{j3} \delta_{c_2 c_3}}{768 \pi^2 (x_1^2 - 1)^4 (x_j^2 - 1)^4 c_w M_W^2 s_w^3} \\
& (-12x_1^2 \log(x_1) (x_1^2 (-2c_w^2 + 2s_w^2 - 1) + x_1^4 (6c_w^2 - 1) + 1) \\
& (x_j^2 - 1)^4 + (x_1^2 - 1) (12(x_1^2 - 1)^3 x_j^2 \log(x_j) \\
& (x_j^2 (-2c_w^2 + 2s_w^2 - 1) + x_j^4 (6c_w^2 - 1) + 1) - (x_1^2 - x_j^2) \\
& (x_j^2 - 1) (10 - 17x_1^2 + x_1^4 - 17x_j^2 + 22x_1^2 x_j^2 + 7x_1^4 x_j^2 + x_j^4 + \\
& 7x_1^2 x_j^4 - 14x_1^4 x_j^4 + 2s_w^2 (2 + 5x_j^2 - x_j^4 + x_1^4 (2x_j^4 + 5x_j^2 - 1) + \\
& x_1^2 (5x_j^4 - 22x_j^2 + 5)) + 2c_w^2 (-5 + 10x_j^2 + 7x_j^4 + \\
& (31x_j^4 - 26x_j^2 + 7) x_1^4 - 2(13x_j^4 + 4x_j^2 - 5) x_1^2)) , \tag{B.11}
\end{aligned}$$

$$\begin{aligned}
(M_{c_2, c_3}^{1, Z})_R = & \sum_{j=2}^3 \frac{ie^3 m_b \varepsilon_Z (V_{\text{CKM}}^{j2})^* V_{\text{CKM}}^{j3} \delta_{c_2 c_3}}{768 \pi^2 (x_1^2 - 1)^4 (x_j^2 - 1)^4 c_w M_W^2 s_w^3} \\
& (-12x_1^2 \log(x_1) (x_1^2 (-2c_w^2 + 2s_w^2 - 1) + x_1^4 (6c_w^2 - 1) + 1) \\
& (x_j^2 - 1)^4 + (x_1^2 - 1) (12(x_1^2 - 1)^3 x_j^2 \log(x_j) \\
& (x_j^2 (-2c_w^2 + 2s_w^2 - 1) + x_j^4 (6c_w^2 - 1) + 1) - (x_1^2 - x_j^2) \\
& (x_j^2 - 1) (10 - 17x_1^2 + x_1^4 - 17x_j^2 + 22x_1^2 x_j^2 + 7x_1^4 x_j^2 + x_j^4 + \\
& 7x_1^2 x_j^4 - 14x_1^4 x_j^4 + 2s_w^2 (2 + 5x_j^2 - x_j^4 + x_1^4 (2x_j^4 + 5x_j^2 - 1) + \\
& x_1^2 (5x_j^4 - 22x_j^2 + 5)) + 2c_w^2 (-5 + 10x_j^2 + 7x_j^4 + \\
& (31x_j^4 - 26x_j^2 + 7) x_1^4 - 2(13x_j^4 + 4x_j^2 - 5) x_1^2)) . \tag{B.12}
\end{aligned}$$

The Wilson coefficients for $b \rightarrow dZ_D$ and $d \rightarrow sZ_D$ can be obtained by changing the CKM matrix elements and the masses of the incoming and outgoing quarks in the equations above.

References

- [1] B. Holdom, *Two U(1)'s and Epsilon Charge Shifts*, *Phys. Lett. B* **166** (1986) 196.
- [2] S. Gopalakrishna, S. Jung and J.D. Wells, *Higgs boson decays to four fermions through an abelian hidden sector*, *Phys. Rev. D* **78** (2008) 055002 [[0801.3456](#)].
- [3] H. Davoudiasl, H.-S. Lee and W.J. Marciano, *'Dark' Z implications for Parity Violation, Rare Meson Decays, and Higgs Physics*, *Phys. Rev. D* **85** (2012) 115019 [[1203.2947](#)].
- [4] A. Datta, J. Liao and D. Marfatia, *A light Z' for the R_K puzzle and nonstandard neutrino interactions*, *Phys. Lett. B* **768** (2017) 265 [[1702.01099](#)].
- [5] F. Sala and D.M. Straub, *A New Light Particle in B Decays?*, *Phys. Lett. B* **774** (2017) 205 [[1704.06188](#)].
- [6] F. Bishara, U. Haisch and P.F. Monni, *Regarding light resonance interpretations of the B decay anomalies*, *Phys. Rev. D* **96** (2017) 055002 [[1705.03465](#)].

- [7] D. Ghosh, *Explaining the R_K and R_{K^*} anomalies*, *Eur. Phys. J. C* **77** (2017) 694 [[1704.06240](#)].
- [8] A. Datta, J. Kumar, J. Liao and D. Marfatia, *New light mediators for the R_K and R_{K^*} puzzles*, *Phys. Rev. D* **97** (2018) 115038 [[1705.08423](#)].
- [9] W. Altmannshofer, M.J. Baker, S. Gori, R. Harnik, M. Pospelov, E. Stamou et al., *Light resonances and the low- q^2 bin of R_{K^*}* , *JHEP* **03** (2018) 188 [[1711.07494](#)].
- [10] A. Datta, B. Dutta, S. Liao, D. Marfatia and L.E. Strigari, *Neutrino scattering and B anomalies from hidden sector portals*, *JHEP* **01** (2019) 091 [[1808.02611](#)].
- [11] A. Datta, J. Kumar and D. London, *The B anomalies and new physics in $b \rightarrow se^+e^-$* , *Phys. Lett. B* **797** (2019) 134858 [[1903.10086](#)].
- [12] L. Darmé, M. Fedele, K. Kowalska and E.M. Sessolo, *Flavour anomalies from a split dark sector*, *JHEP* **08** (2020) 148 [[2002.11150](#)].
- [13] D. Borah, L. Mukherjee and S. Nandi, *Low scale $U(1)_X$ gauge symmetry as an origin of dark matter, neutrino mass and flavour anomalies*, *JHEP* **12** (2020) 052 [[2007.13778](#)].
- [14] L. Darmé, M. Fedele, K. Kowalska and E.M. Sessolo, *Flavour anomalies and the muon $g - 2$ from feebly interacting particles*, *JHEP* **03** (2022) 085 [[2106.12582](#)].
- [15] A. Crivellin, C.A. Manzari, W. Altmannshofer, G. Inguglia, P. Feichtinger and J. Martin Camalich, *Towards excluding a light Z' explanation of $b \rightarrow s\ell^+\ell^-$* , [2202.12900](#).
- [16] F. Xu, *Dark Z Implication for Flavor Physics*, *JHEP* **06** (2015) 170 [[1504.07415](#)].
- [17] E.J. Chun, J.-C. Park and S. Scopel, *Dark matter and a new gauge boson through kinetic mixing*, *JHEP* **02** (2011) 100 [[1011.3300](#)].
- [18] E. Bertuzzo, S. Jana, P.A.N. Machado and R. Zukanovich Funchal, *Neutrino Masses and Mixings Dynamically Generated by a Light Dark Sector*, *Phys. Lett. B* **791** (2019) 210 [[1808.02500](#)].
- [19] E. Bertuzzo, S. Jana, P.A.N. Machado and R. Zukanovich Funchal, *Dark Neutrino Portal to Explain MiniBooNE excess*, *Phys. Rev. Lett.* **121** (2018) 241801 [[1807.09877](#)].
- [20] J.M. Link and X.-J. Xu, *Searching for BSM neutrino interactions in dark matter detectors*, *JHEP* **08** (2019) 004 [[1903.09891](#)].
- [21] A.V. Bednyakov and c.H. TanyıLdıZı, *A Mathematica Package for Calculation of One-Loop Penguins in FCNC Processes*, *Int. J. Mod. Phys. C* **26** (2014) 1550042 [[1311.5546](#)].
- [22] J.J. Sakurai, *Theory of strong interactions*, *Annals Phys.* **11** (1960) 1.
- [23] N.M. Kroll, T.D. Lee and B. Zumino, *Neutral Vector Mesons and the Hadronic Electromagnetic Current*, *Phys. Rev.* **157** (1967) 1376.
- [24] T.D. Lee and B. Zumino, *Field Current Identities and Algebra of Fields*, *Phys. Rev.* **163** (1967) 1667.
- [25] H. Fraas and D. Schildknecht, *Vector-meson dominance and diffractive electroproduction of vector mesons*, *Nucl. Phys. B* **14** (1969) 543.
- [26] M. Bando, T. Kugo, S. Uehara, K. Yamawaki and T. Yanagida, *Is rho Meson a Dynamical Gauge Boson of Hidden Local Symmetry?*, *Phys. Rev. Lett.* **54** (1985) 1215.
- [27] S. Tulin, *New weakly-coupled forces hidden in low-energy QCD*, *Phys. Rev. D* **89** (2014) 114008 [[1404.4370](#)].

- [28] P. Ilten, Y. Soreq, M. Williams and W. Xue, *Serendipity in dark photon searches*, *JHEP* **06** (2018) 004 [[1801.04847](#)].
- [29] A.L. Foguel, P. Reimitz and R.Z. Funchal, *A robust description of hadronic decays in light vector mediator models*, *JHEP* **04** (2022) 119 [[2201.01788](#)].
- [30] PARTICLE DATA GROUP collaboration, *Review of Particle Physics*, *PTEP* **2022** (2022) 083C01.
- [31] M. Artuso, G. Borissov and A. Lenz, *CP violation in the B_s^0 system*, *Rev. Mod. Phys.* **88** (2016) 045002 [[1511.09466](#)].
- [32] T. Inami and C.S. Lim, *Effects of Superheavy Quarks and Leptons in Low-Energy Weak Processes $k(L) \rightarrow \mu \text{ anti-}\mu$, $K^+ \rightarrow \pi^+ \text{ Neutrino anti-neutrino}$ and $K^0 \leftrightarrow \text{anti-}K^0$* , *Prog. Theor. Phys.* **65** (1981) 297.
- [33] FERMILAB LATTICE, MILC collaboration, *$B_{(s)}^0$ -mixing matrix elements from lattice QCD for the Standard Model and beyond*, *Phys. Rev. D* **93** (2016) 113016 [[1602.03560](#)].
- [34] G. Buchalla, A.J. Buras and M.E. Lautenbacher, *Weak decays beyond leading logarithms*, *Rev. Mod. Phys.* **68** (1996) 1125 [[hep-ph/9512380](#)].
- [35] Y. Aoki et al., *FLAG Review 2021*, [2111.09849](#).
- [36] L. Di Luzio, M. Kirk, A. Lenz and T. Rauh, *ΔM_s theory precision confronts flavour anomalies*, *JHEP* **12** (2019) 009 [[1909.11087](#)].
- [37] FLAVOUR LATTICE AVERAGING GROUP collaboration, *FLAG Review 2019: Flavour Lattice Averaging Group (FLAG)*, *Eur. Phys. J. C* **80** (2020) 113 [[1902.08191](#)].
- [38] W. Altmannshofer and P. Stangl, *New physics in rare B decays after Moriond 2021*, *Eur. Phys. J. C* **81** (2021) 952 [[2103.13370](#)].
- [39] D. Guadagnoli, C. Langenbruch and E. Manoni, *WG3 Summary – Rare B, D and K decays, in 11th International Workshop on the CKM Unitarity Triangle*, 4, 2022 [[2204.03942](#)].
- [40] LHCb collaboration, *Measurement of the $B_s^0 \rightarrow \mu^+ \mu^-$ decay properties and search for the $B^0 \rightarrow \mu^+ \mu^-$ and $B_s^0 \rightarrow \mu^+ \mu^- \gamma$ decays*, *Phys. Rev. D* **105** (2022) 012010 [[2108.09283](#)].
- [41] K. Fuyuto, W.-S. Hou and M. Kohda, *Z' -induced FCNC decays of top, beauty, and strange quarks*, *Phys. Rev. D* **93** (2016) 054021 [[1512.09026](#)].
- [42] P. Ball and R. Zwicky, *$B_{d,s} \rightarrow \rho, \omega, K^*, \phi$ decay form-factors from light-cone sum rules revisited*, *Phys. Rev. D* **71** (2005) 014029 [[hep-ph/0412079](#)].
- [43] T. Felkl, S.L. Li and M.A. Schmidt, *A tale of invisibility: constraints on new physics in $b \rightarrow s\nu$* , *JHEP* **12** (2021) 118 [[2111.04327](#)].
- [44] BELLE-II collaboration, *Search for $B^+ \rightarrow K^+ \nu \bar{\nu}$ decays with an inclusive tagging method at the Belle II experiment*, in *55th Rencontres de Moriond on Electroweak Interactions and Unified Theories*, 5, 2021 [[2105.05754](#)].
- [45] BELLE collaboration, *Search for $B \rightarrow h\nu\bar{\nu}$ decays with semileptonic tagging at Belle*, *Phys. Rev. D* **96** (2017) 091101 [[1702.03224](#)].
- [46] NA62 collaboration, *Measurement of the very rare $K^+ \rightarrow \pi^+ \nu \bar{\nu}$ decay*, *JHEP* **06** (2021) 093 [[2103.15389](#)].
- [47] KOTO collaboration, *Study of the $K_L \rightarrow \pi^0 \nu \bar{\nu}$ Decay at the J-PARC KOTO Experiment*, *Phys. Rev. Lett.* **126** (2021) 121801 [[2012.07571](#)].

- [48] A.J. Buras, D. Buttazzo, J. Girrbach-Noe and R. Knegjens, $K^+ \rightarrow \pi^+ \nu \bar{\nu}$ and $K_L \rightarrow \pi^0 \nu \bar{\nu}$ in the Standard Model: status and perspectives, *JHEP* **11** (2015) 033 [[1503.02693](#)].
- [49] PARTICLE DATA GROUP collaboration, *Review of Particle Physics*, .
- [50] Y. Grossman and Y. Nir, $K(L) \rightarrow \pi^0$ neutrino anti-neutrino beyond the standard model, *Phys. Lett. B* **398** (1997) 163 [[hep-ph/9701313](#)].
- [51] NA62 collaboration, Search for K^+ decays to a muon and invisible particles, *Phys. Lett. B* **816** (2021) 136259 [[2101.12304](#)].
- [52] A.A. Poblaguev et al., Experimental study of the radiative decays $K^+ \rightarrow \mu^+ \nu e^+ e^-$ and $K^+ \rightarrow e^+ \nu e^+ e^-$, *Phys. Rev. Lett.* **89** (2002) 061803 [[hep-ex/0204006](#)].
- [53] PIENU collaboration, Search for three body pion decays $\pi^+ \rightarrow l^+ \nu X$, *Phys. Rev. D* **103** (2021) 052006 [[2101.07381](#)].
- [54] QWEAK collaboration, Precision measurement of the weak charge of the proton, *Nature* **557** (2018) 207 [[1905.08283](#)].
- [55] C.S. Wood, S.C. Bennett, D. Cho, B.P. Masterson, J.L. Roberts, C.E. Tanner et al., Measurement of parity nonconservation and an anapole moment in cesium, *Science* **275** (1997) 1759.
- [56] M. Cadeddu, N. Cargioli, F. Dordei, C. Giunti and E. Picciau, Muon and electron $g-2$ and proton and cesium weak charges implications on dark Zd models, *Phys. Rev. D* **104** (2021) 011701 [[2104.03280](#)].
- [57] CHARM-II collaboration, First observation of neutrino trident production, *Phys. Lett. B* **245** (1990) 271.
- [58] CCFR collaboration, Neutrino tridents and W Z interference, *Phys. Rev. Lett.* **66** (1991) 3117.
- [59] W. Altmannshofer, S. Gori, J. Martín-Albo, A. Sousa and M. Wallbank, Neutrino Tridents at DUNE, *Phys. Rev. D* **100** (2019) 115029 [[1902.06765](#)].
- [60] COHERENT collaboration, Observation of Coherent Elastic Neutrino-Nucleus Scattering, *Science* **357** (2017) 1123 [[1708.01294](#)].
- [61] COHERENT collaboration, First Measurement of Coherent Elastic Neutrino-Nucleus Scattering on Argon, *Phys. Rev. Lett.* **126** (2021) 012002 [[2003.10630](#)].
- [62] COHERENT collaboration, COHERENT Collaboration data release from the first detection of coherent elastic neutrino-nucleus scattering on argon, [2006.12659](#).
- [63] T. Han, J. Liao, H. Liu and D. Marfatia, Nonstandard neutrino interactions at COHERENT, DUNE, T2HK and LHC, *JHEP* **11** (2019) 028 [[1910.03272](#)].
- [64] H. Banerjee, B. Dutta and S. Roy, Probing $L\mu-L\tau$ models with CE ν NS: A new look at the combined COHERENT CsI and Ar data, *Phys. Rev. D* **104** (2021) 015015 [[2103.10196](#)].
- [65] M. Atzori Corona, M. Cadeddu, N. Cargioli, F. Dordei, C. Giunti, Y.F. Li et al., Probing light mediators and $(g-2)_\mu$ through detection of coherent elastic neutrino nucleus scattering at COHERENT, *JHEP* **05** (2022) 109 [[2202.11002](#)].
- [66] ATLAS collaboration, Measurements of Four-Lepton Production at the Z Resonance in pp Collisions at $\sqrt{s} = 7$ and 8 TeV with ATLAS, *Phys. Rev. Lett.* **112** (2014) 231806 [[1403.5657](#)].

- [67] ATLAS collaboration, *Search for a new Z' gauge boson in 4μ events with the ATLAS experiment*, .
- [68] CMS collaboration, *Observation of Z Decays to Four Leptons with the CMS Detector at the LHC*, *JHEP* **12** (2012) 034 [[1210.3844](#)].
- [69] CMS collaboration, *Search for an $L_\mu - L_\tau$ gauge boson using $Z \rightarrow 4\mu$ events in proton-proton collisions at $\sqrt{s} = 13$ TeV*, *Phys. Lett. B* **792** (2019) 345 [[1808.03684](#)].
- [70] BELLE-II collaboration, *Search for an Invisibly Decaying Z' Boson at Belle II in $e^+e^- \rightarrow \mu^+\mu^-(e^\pm\mu^\mp)$ Plus Missing Energy Final States*, *Phys. Rev. Lett.* **124** (2020) 141801 [[1912.11276](#)].
- [71] LHCb collaboration, *Search for $A' \rightarrow \mu^+\mu^-$ Decays*, *Phys. Rev. Lett.* **124** (2020) 041801 [[1910.06926](#)].
- [72] LHCb collaboration, *Measurements of the S -wave fraction in $B^0 \rightarrow K^+\pi^-\mu^+\mu^-$ decays and the $B^0 \rightarrow K^*(892)^0\mu^+\mu^-$ differential branching fraction*, *JHEP* **11** (2016) 047 [[1606.04731](#)].
- [73] LHCb collaboration, *Differential branching fractions and isospin asymmetries of $B \rightarrow K^{(*)}\mu^+\mu^-$ decays*, *JHEP* **06** (2014) 133 [[1403.8044](#)].
- [74] LHCb collaboration, *Branching Fraction Measurements of the Rare $B_s^0 \rightarrow \phi\mu^+\mu^-$ and $B_s^0 \rightarrow f_2'(1525)\mu^+\mu^-$ Decays*, *Phys. Rev. Lett.* **127** (2021) 151801 [[2105.14007](#)].
- [75] BELLE collaboration, *Test of lepton flavor universality and search for lepton flavor violation in $B \rightarrow K\ell\ell$ decays*, *JHEP* **03** (2021) 105 [[1908.01848](#)].
- [76] LHCb collaboration, *Measurement of the $B^0 \rightarrow K^{*0}e^+e^-$ branching fraction at low dilepton mass*, *JHEP* **05** (2013) 159 [[1304.3035](#)].
- [77] BABAR collaboration, *Measurement of the $B \rightarrow X_s l^+ l^-$ branching fraction and search for direct CP violation from a sum of exclusive final states*, *Phys. Rev. Lett.* **112** (2014) 211802 [[1312.5364](#)].
- [78] LHCb collaboration, *Measurement of lepton universality parameters in $B^+ \rightarrow K^+\ell^+\ell^-$ and $B^0 \rightarrow K^{*0}\ell^+\ell^-$ decays*, [2212.09153](#).
- [79] D.M. Straub, *flavio: a Python package for flavour and precision phenomenology in the Standard Model and beyond*, [1810.08132](#).
- [80] MUON G-2 collaboration, *Final Report of the Muon E821 Anomalous Magnetic Moment Measurement at BNL*, *Phys. Rev. D* **73** (2006) 072003 [[hep-ex/0602035](#)].
- [81] MUON G-2 collaboration, *Measurement of the Positive Muon Anomalous Magnetic Moment to 0.46 ppm*, *Phys. Rev. Lett.* **126** (2021) 141801 [[2104.03281](#)].
- [82] T. Aoyama et al., *The anomalous magnetic moment of the muon in the Standard Model*, *Phys. Rept.* **887** (2020) 1 [[2006.04822](#)].
- [83] M. Lindner, M. Platscher and F.S. Queiroz, *A Call for New Physics : The Muon Anomalous Magnetic Moment and Lepton Flavor Violation*, *Phys. Rept.* **731** (2018) 1 [[1610.06587](#)].
- [84] A. Bharucha, D.M. Straub and R. Zwicky, *$B \rightarrow V\ell^+\ell^-$ in the Standard Model from light-cone sum rules*, *JHEP* **08** (2016) 098 [[1503.05534](#)].
- [85] J. Lyon and R. Zwicky, *Isospin asymmetries in $B \rightarrow (K^*, \rho)\gamma/l^+l^-$ and $B \rightarrow K l^+l^-$ in and beyond the standard model*, *Phys. Rev. D* **88** (2013) 094004 [[1305.4797](#)].

- [86] P. Ball and R. Zwicky, *New results on $B \rightarrow \pi, K, \eta$ decay formfactors from light-cone sum rules*, *Phys. Rev. D* **71** (2005) 014015 [[hep-ph/0406232](#)].
- [87] Y.-f. Wu and D.-X. Zhang, *On Unparticles and $K^+ \rightarrow \pi^+ + \text{Missing Energy}$* , [0712.3923](#).
- [88] J. Gao and B.A. Li, *Form-factors of pion and kaon*, *Phys. Rev. D* **61** (2000) 113006 [[hep-ph/9911438](#)].
- [89] J. Bijnens and A. Khodjamirian, *Exploring light cone sum rules for pion and kaon form-factors*, *Eur. Phys. J. C* **26** (2002) 67 [[hep-ph/0206252](#)].
- [90] F. Mescia, C. Smith and S. Trine, *$K(L) \rightarrow \pi^0 e + e^-$ and $K(L) \rightarrow \pi^0 \mu + \mu^-$: A Binary star on the stage of flavor physics*, *JHEP* **08** (2006) 088 [[hep-ph/0606081](#)].
- [91] KTeV collaboration, *Measurements of semileptonic $K(L)$ decay form-factors*, *Phys. Rev. D* **70** (2004) 092007 [[hep-ex/0406003](#)].
- [92] NA48 collaboration, *Measurement of $K0(e3)$ form-factors*, *Phys. Lett. B* **604** (2004) 1 [[hep-ex/0410065](#)].
- [93] O.P. Yushchenko et al., *High statistic study of the $K^- \rightarrow \pi^0 \mu^- \nu$ decay*, *Phys. Lett. B* **581** (2004) 31 [[hep-ex/0312004](#)].
- [94] KLOE collaboration, *Measurement of the form-factor slopes for the decay $K(L) \rightarrow \pi^\pm e^\mp \nu$ with the KLOE detector*, *Phys. Lett. B* **636** (2006) 166 [[hep-ex/0601038](#)].
- [95] W.J. Marciano and Z. Parsa, *Rare kaon decays with “missing energy”*, *Phys. Rev. D* **53** (1996) R1.
- [96] H. Leutwyler and M. Roos, *Determination of the Elements $V(us)$ and $V(ud)$ of the Kobayashi-Maskawa Matrix*, *Z. Phys. C* **25** (1984) 91.
- [97] D. Becirevic, G. Isidori, V. Lubicz, G. Martinelli, F. Mescia, S. Simula et al., *The $K \rightarrow \pi$ vector form-factor at zero momentum transfer on the lattice*, *Nucl. Phys. B* **705** (2005) 339 [[hep-ph/0403217](#)].
- [98] C. Dawson, T. Izubuchi, T. Kaneko, S. Sasaki and A. Soni, *$K(l3)$ form-factor with two-flavors of dynamical domain-wall quarks*, *PoS LAT2005* (2006) 337 [[hep-lat/0510018](#)].
- [99] JLQCD collaboration, *Kaon semileptonic decay form-factors in two-flavor QCD*, *PoS LAT2005* (2006) 357 [[hep-lat/0510068](#)].
- [100] G. Buchalla, G. D’Ambrosio and G. Isidori, *Extracting short distance physics from $K(L,S) \rightarrow \pi^0 e + e^-$ decays*, *Nucl. Phys. B* **672** (2003) 387 [[hep-ph/0308008](#)].